




Recent advances on support materials for enhanced Pt-based catalysts: applications in oxygen reduction reactions for electrochemical energy storage

Feng Zhan¹, Lingyun Huang¹, Yue Luo¹, MUYANG Chen², Rui Tan^{2,*}, Xinhua Liu^{3,*}, Gang Liu⁴, and Zhiming Feng^{5,*} 

¹ School of Resources, Environment and Materials Science, Guangxi University, Nanning 530004, China

² Department of Chemical Engineering, Swansea University, Swansea SA1 8EN, UK

³ School of Transportation Science and Engineering, Beihang University, Beijing 100191, China

⁴ IDTECH (Suzhou) Co., Ltd., Suzhou 215217, China

⁵ School of Chemical Engineering, The University of Manchester, Manchester M13 9PL, UK

Received: 25 September 2024

Accepted: 2 January 2025

Published online:

15 January 2025

© The Author(s), 2025

ABSTRACT

As the demand for sustainable energy solutions grows, developing efficient energy conversion and storage technologies, such as fuel cells and metal-air batteries, is vital. Oxygen Reduction Reaction (ORR) is a significant limitation in electrochemical systems due to its slower kinetics. Although Pt-based catalysts are commonly used to address this challenge, their high cost and suboptimal performance remain significant obstacles to further development. This review offers a comprehensive overview of advanced support materials aimed at improving the efficiency, durability, and cost-effectiveness of Pt-based catalysts. By examining a range of materials, including mesoporous carbon, graphene, carbon nanotubes, and metal oxides, the review clarifies the relationship between the structural properties of these supports and their influence on ORR performance. Additionally, it discusses the fundamental characteristics of these materials, their practical applications in fuel cells, and explores potential solutions and future directions for optimizing Pt-based catalysts to advance sustainable energy conversion technologies. Future research could focus on nano-engineering and composite material development to unlock the full potential of Pt-based catalysts, significantly enhancing their economic viability and performance in energy applications.

Handling Editor: Pedro Camargo.

Address correspondence to E-mail: rui.tan@swansea.ac.uk; liuxinhua19@buaa.edu.cn; zhiming.feng@manchester.ac.uk

<https://doi.org/10.1007/s10853-025-10606-1>

Introduction

Renewable energy technologies are essential for achieving global net-zero emissions targets, providing sustainable alternatives to conventional energy sources that often result in significant carbon emissions, environmental damage, and the depletion of natural resources [1–5]. Among these technologies, electrochemical energy systems such as fuel cells and metal-air batteries play a crucial role in energy conversion and storage due to their high efficiency and low environmental impact [6–9]. The Oxygen Reduction Reaction (ORR) is fundamental to electrochemical energy systems, particularly in fuel cells and metal-air batteries, where it underpins the cathodic process [10, 11]. For example, Fuel cells (FCs) play a pivotal role in addressing global energy challenges, particularly in the pursuit of net zero emissions [12, 13]. By providing efficient, sustainable, and scalable energy conversion technologies, fuel cells are integral to the transition towards greener energy systems. They offer significant advantages over conventional energy technologies, including higher efficiency, reduced environmental impact, and the ability to utilize diverse fuel sources [14]. Emphasizing the importance of advancing fuel cell technology is crucial for meeting the growing demands for clean energy solutions and achieving the ambitious goals set for carbon neutrality [15]. FCs are electrochemical energy conversion devices that generate electricity through reactions between fuel and oxidants [16–18]. A typical H₂-O₂ fuel cell uses hydrogen as the fuel and oxygen as the oxidant. In this system, the hydrogen oxidation reaction (HOR) occurs at the anode, while the ORR takes place at the cathode. The ORR is notoriously slow, with a typical reaction current of 1×10^{-10} mA•cm⁻², which is substantially slower, seven orders of magnitude lower than that of the HOR at the current of 1×10^{-3} mA cm⁻². This significant difference underscores the ORR's crucial impact on the overall efficiency and effectiveness of the fuel cell, making it a decisive step in the energy conversion process [19–21]. Consequently, extensive research has been focused on enhancing the performance of cathode catalysts to address the bottleneck [18, 22, 23].

Electrocatalysts offer several advantages over traditional chemical catalysts, including higher energy efficiency as they operate at lower temperatures, greater selectivity that minimizes unwanted byproducts, and a reduced environmental impact [24, 25]. These benefits make them particularly valuable in renewable energy

applications, such as water splitting and carbon dioxide reduction, facilitating the integration and storage of renewable energy. Additionally, electrocatalysts tend to be more reusable and stable, enhancing their practicality for long-term industrial processes [26–28]. Besides, recent studies have underscored the significance of anion vacancies in improving the electrocatalytic efficiency of water splitting technologies. These vacancies enhance the adsorption and dissociation of water molecules, critical for efficient H₂ and O₂ production [29]. By altering the electronic structure of catalysts, anion vacancies reduce the overpotential required for both the OER and hydrogen evolution reaction (HER), thus boosting energy efficiency and catalyst stability. This introduction briefly reviews key findings on the role of anion vacancies in water electrolysis, highlighting their impact on advancing sustainable hydrogen production [30]. Among various catalysts, platinum (Pt) and its alloys are distinguished for their superior catalytic properties, significantly lowering overpotentials in the ORR and enhancing energy efficiency [31]. Pt-based electrodes are crucial for catalyzing the Oxygen Reduction Reaction (ORR) in fuel cells, yet they face significant challenges including susceptibility to poisoning by carbon monoxide, which inhibits catalytic activity, high costs due to platinum's scarcity, and durability concerns under operational conditions [32, 33]. Despite these drawbacks, the advantages of Pt-based electrodes, such as their unmatched catalytic efficiency, exceptional electrochemical stability, and improved scalability through nanostructuring make them indispensable in advancing fuel cell technology [34]. The extensive use of Pt-based catalysts is limited by their high cost, scarcity, and decreased durability under the demanding conditions of fuel cell operations [35, 36]. Furthermore, the cathode typically requires three to five times more platinum than the anode, underscoring the urgent need for more efficient and sustainable catalytic alternatives. In the production of fuel cells, Pt-based catalysts represent a significant cost component, accounting for 30–45% of the total expenses [37]. To mitigate these costs and enhance ORR efficiency, considerable research has been directed towards innovative catalyst solutions, including the development of non-precious metal catalysts, transition metal-nitrogen-carbon (M-N-C) catalysts [38–40], and novel catalyst structures that reduce Pt content [41, 42]. For example, doping non-precious metals, such as 3d transition metals (Fe, Co, and Ni) into Pt is an effective method [43–45]. These Pt-based catalyst nanoparticles not only reduce Pt but also exhibit unprecedented

electrocatalytic performance by enhancing the activity and stability of ORR kinetics through unique electronic effects [46, 47]. In addition to modifying catalyst components, advanced catalyst structures, such as core–shell structures [48], hollow structure [49, 50], nanomaterial structures [51], etc. By controlling the size of the Pt nanoparticles, the reaction surface area of the Pt-based cathode catalyst can be fully utilized, thereby reducing ORR to a level that is not hindered by specific activities. Building on these developments, single-atom catalysts (SACs) have also emerged as a significant advancement [52]. These catalysts optimize the use of precious metals like platinum by dispersing individual atoms on suitable supports, such as graphene or nitrogen-doped carbon. This atomic dispersion maximizes the active surface area and enhances electrochemical performance, particularly in ORR [53, 54].

Recent advancements in support materials have enabled the creation of innovative designs, such as core–shell, hollow, and nanomaterial structures [55]. These sophisticated configurations maximize the active surface area of Pt nanoparticles, enhance stability, and boost the efficiency of catalytic processes, making them vital for the development of more effective and sustainable fuel cell technologies.

This review provides a comprehensive overview of recent advancements in support materials for Pt-based catalysts, elucidating the relationship between their structural properties and enhanced electrochemical performance, particularly under acidic conditions. Focusing on Pt-based electrocatalysts, this examination highlights their comparatively higher ORR activity and stability in the acidic and oxidizing environments of PEMFC cathodes. Mechanistic insights into these catalytic support materials and their practical applications in fuel cells will also be explored. Furthermore, the review discusses prospective solutions and future directions for developing novel support materials to improve the efficiency of Pt-based catalysts, ultimately bringing PEMFCs closer to commercial application.

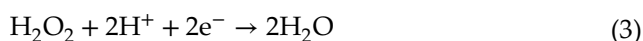
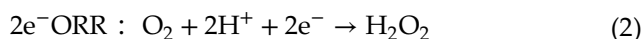
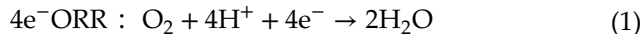
Fundamentals of oxygen reduction reaction

ORR is a process where oxygen molecules accept electrons to be converted into water or hydroxide ions. The efficiency and rate of this reaction impacts the performance and efficiency of batteries. The kinetics of ORR

are complex, and the reaction pathways and products are influenced by the properties of the electrode materials, the activity of catalysts, and the properties of the electrolyte. As aforementioned, cathode catalysts typically require a higher loading of Pt compared to anode catalysts [56, 57]. To better evaluate catalytic behavior and understand ORR properties, physical, chemical and electrochemical characterization methods are generally combined to provide reliable metrics.

Reaction mechanism

In an acidic electrolyte, there are two main possible pathways for the ORR process at varied standard potentials [58]. One is a fast one-step four-electron ($4e^-$) pathway with a constant electrode potential $E_0 = 1.23$ V, where each oxygen molecule acquires $4e^-$ to produce water. The other is a slow two-step two-electron ($2e^-$) pathway with a stand electrode potential $E_0 = 0.682$ V, where each oxygen molecule acquires $2e^-$ to produce H_2O_2 . The overall charge transfer reaction depends on the chemistry of the electrolyte. The mechanisms of the 2- and 4-electron pathways are as follows.



The electrochemical reaction of a fuel cell is determined by the ORR at the cathode. In fuel cell applications, it is important to avoid the $2e^-$ pathway and achieve the efficient $4e^-$ pathway to maximize fuel cell performance.

In the ORR, the rate-determining step (RDS) is the slowest step of the reaction process that controls the overall reaction rate [59]. ORR can proceed through different electron transfer pathways, including four-electron and two-electron pathways. Understanding which step acts as the rate-determining step is crucial for designing more effective catalysts and improving reaction efficiency [60]. For example, in the four-electron pathway of reactions, the rate-determining step varies with the pH of the solution: in alkaline conditions, the reduction of hydrogen peroxide to water tends to be the rate-determining step, whereas in acidic solutions, the transfer of the first electron generally acts as the limiting step.

For ORR, kinetic barriers represent critical energy thresholds that must be surpassed to advance the reaction, directly influencing the reaction's rate [61]. These barriers are often related to the rate-determining steps discussed earlier. Specifically, in the ORR, such barriers can encompass the energy required for electron transfer, the adsorption and desorption processes at the catalyst's active sites, and the stability and conversion efficiency of reaction intermediates [62]. Each of these factors plays a significant role in determining how efficiently and quickly the reaction proceeds.

To effectively address the kinetic barriers in catalytic reactions, such as those encountered in the ORR, a variety of strategies can be adopted [63]. These approaches are designed to enhance reaction kinetics and overall efficiency by tackling the challenges at the molecular level. For instance, catalyst design is crucial; developing new catalysts like alloys, single-atom catalysts, or non-precious metal catalysts can provide more active sites and facilitate better electron and proton transfers. Surface modification of catalysts, through techniques like increasing surface roughness or introducing functional groups, can also significantly enhance adsorption and desorption capabilities, effectively lowering the energy barriers associated with these processes [64]. Additionally, the use of additives can alter electrolyte properties and improve interactions at the electrolyte–electrode interface, thereby boosting the reaction rate and efficiency. Lastly, optimizing the electrode design, such as employing porous or three-dimensional structures, can increase the effective surface area available for reactions, thereby enhancing the reaction rates. These integrated strategies help surmount the kinetic barriers, paving the way for more efficient catalytic processes [65].

Figure 1 displays the ORR activity of various metal catalysts as a function of their changes in standard electrode potential (ΔE_0), derived from Density Functional Theory (DFT) calculations [66]. DFT is a widely used computational method for predicting and analyzing the energy properties of materials. The volcano plot reveals that Pt achieves peak ORR activity at an optimal oxygen binding energy. DFT analyses provide detailed insights, showing that a Pt monolayer on Ni, Co, or Fe substrates results in oxygen binding energies of 1.89 eV, 2.00 eV, and 2.06 eV, respectively. Such variations indicate that altering Pt's surface composition significantly impacts its catalytic performance. Particularly, a Pt skin on a Pt₃Co(111) substrate has an oxygen binding energy that

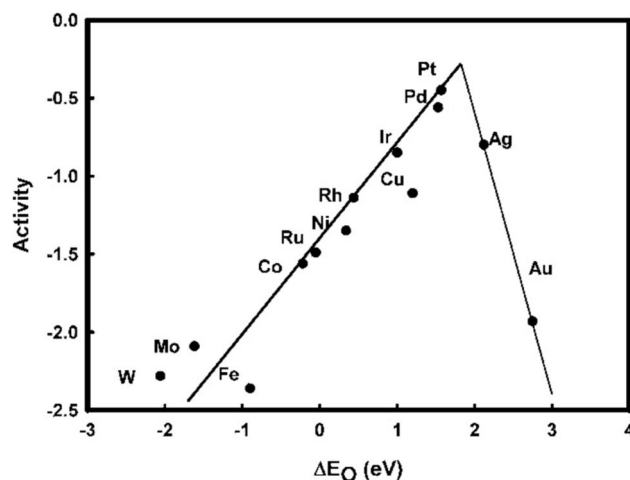


Figure 1 Volcano-type correlation of ORR activity with oxygen-binding energy across different metal catalysts in alkaline media. Reproduced with permission from reference [66]. Copyright 2004, American Chemical Society.

is 0.38 eV lower than that on pure Pt(111), which is associated with enhanced ORR activity, as corroborated by experimental results [67].

Electrochemical properties and evaluation techniques

Electrochemical properties can be tested in three-electrode electrochemical cells using various methods, such as cyclic voltammetry (CV) and linear scanning voltammetry (LSV) [68]. The polarization curves of the catalysts can be obtained by LSV, where the half-wave potential ($E_{1/2}$) of these curves indicates the ORR kinetics of the catalysts. ORR activity is usually calculated using LSV measurements. ORR activity can be described by mass activity (A/mg_{Pt})—activity per unit of catalyst mass, indicating effective utilization of the catalyst material; and specific activity (mA/cm^2)—activity per unit electrochemical surface area, indicating the inherent reactivity per unit area of the catalyst surface. To measure ORR activity, the electrochemical properties of the catalyst layers are objectively evaluated and compared using the Koutecky-Levich Eq. 4.

$$\frac{1}{I} = \frac{1}{I_k} + \frac{1}{0.62nFC_0D_0^{2/3}v^{-1/6}\omega^{1/2}} \quad (4)$$

where I and I_k represent the limiting diffusion current and the kinetically controlled reaction current, respectively; n is the number of electrons transferred in the

reaction; F is the Faraday constant; D_0 is the diffusion coefficient of O_2 in 0.1 M $HClO_4$; C_0 is the oxygen concentration; ν is the kinetic viscosity in 0.1 M $HClO_4$; ω is the rotational angular velocity. The I_k in the formula is corrected before use by the Eq. 5.

$$I_k = \frac{I_{lim} \times I}{I_{lim} - I} \quad (5)$$

For example, when the potential is swept from 0.05 to 1 V vs. RHE, I_{lim} denotes the limiting diffusion current tested at 0.4 V and I denote the limiting diffusion current tested at 0.7 V.

An important parameter in assessing the kinetics of ORR is the Tafel slope (mV/dec). A smaller Tafel slope indicates more significant ORR kinetics. The Tafel slope is calculated from the slope of $E \sim \log |I_k|$ curve using the Tafel analysis and the Koutecky-Levich analysis [69].

$$b = \mp \frac{dE}{d\log|I_k|} \quad (6)$$

where E is the electrode potential; $-$ indicates a reduction reaction and $+$ an oxidation reaction.

Electrochemically active surface area (ECSA) typically degrades over the working life of Pt-based catalysts due to Ostwald ripening, agglomeration of Pt nanoparticles, and corrosion of the carbon support [70]. There are three methods to evaluate ECSA, including CO-stripping [71], cyclic voltammetry via underpotential deposition of hydrogen (H_{upd}) [72] and underpotential deposition of copper (Cu_{upd}) [73]. CO-stripping requires a low concentration of H_2 during operation to avoid the artifact of CO-stripping charge, i.e. CO adsorption on Pt, which inhibits HOR and leads to H_2 accumulation in the cathode, resulting in an error when testing the current. Cu_{upd} cannot make continuous measurements on a single sample because the samples must be cleaned after testing, and it is typically used to determine the Ru content on the surface of Pt-Ru alloys, which is difficult for other Pt-based cathode catalysts and therefore rarely used. Measurements using CV by H_{upd} involve multiple activations at a given scan rate, and then the $ECSA_{Hupd}$ is calculated from the Coulombic charge (Q_h) accumulated during hydrogen uptake and desorption using the equation:

$$ECSA_{Hupd}(cm^2) = \frac{Q_h}{M_{Pt} \times q_h} \quad (7)$$

where M_{Pt} is the mass of metal-loaded Pt on the catalyst and q_h is the charge required to adsorb hydrogen on the platinum surface monolayer.

Typically, H_{upd} test results for ECSA on Pt-based alloy catalysts are lower than these obtained via CO-stripping. This discrepancy is primarily due to contaminants such as O_2 in the gas line, which may react with oxidized surfaces to generate CO, subsequently increasing the detected CO vapor charge and partially overlapping the H_{upd} detection range. Consequently, it is imperative to calibrate the equipment accurately during experimental procedures. In their study, Bruna F et al. [74] assessed the ECSA of Pt/C catalysts using both CO-stripping and H_{upd} techniques within an electrolyte solution of 0.1 mol/L $HClO_4$. They observed that ECSA values derived from CO-stripping were initially higher than those from H_{upd} but exhibited a pronounced decline as the number of cycles increased (Fig. 2a). This decrease in ECSA may be attributed to surface reorganization triggered by the solution polarization of Pt in the presence of CO.

Various methods were used for both physical and electrochemical characterizations. The electrochemical properties of Pt-based catalysts can be evaluated by several techniques, including the rotating disk electrode (RDE), floating electrode technique (FET), and rotating ring disk electrode (RRDE) [75]. Among these, RDE and RRDE are the most widely used due to their good reproducibility and the ease of reaching steady state [76].

The RDE generally consists of a working electrode, a reference electrode (RE) and a counter electrode, immersed in a solution. The solutions can be classified as alkaline and acidic electrolytes [77, 78]. Commonly used alkaline electrolytes are KOH, NaOH, etc. while acidic electrolytes include $HClO_4$, HCl, H_2SO_4 , etc. In acidic conditions, anions can be adsorbed on the active site of catalysts, affecting the ORR performance. To avoid ions interfering with performance and electrical conductivity, high-purity $HClO_4$ with small ion adsorption and moderate concentration (0.1 mol/L) is generally chosen. The $HClO_4$ electrolyte should be replaced frequently, as dilute perchloric acid decomposes over time into Cl^- , which has a stronger adsorption capacity than ClO_4^- [79].

Physical characterization is also crucial for investigating the catalyst morphology, activity and fundamental kinetics under operating conditions. High-precision physical characterizations can be combined with electrochemical techniques, facilitate detailed studies of

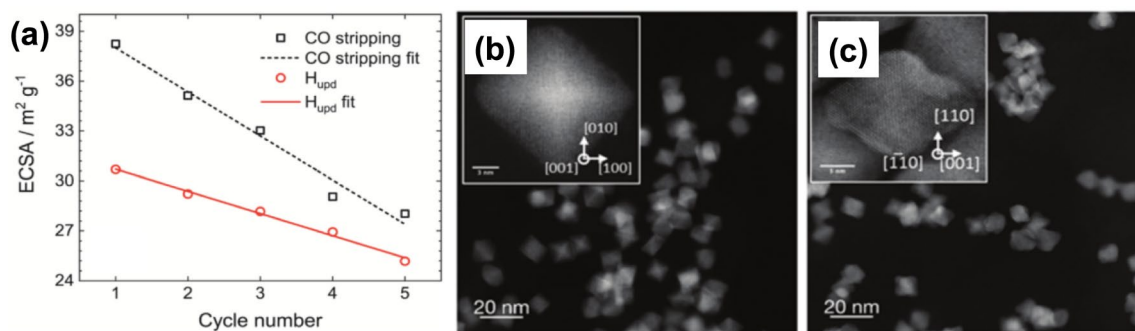


Figure 2 **a** Measurement of ECSA by H_{upd} and CO stripping in 0.1 mol/L HClO_4 electrolyte solution. Reproduced with permission from reference [74]. Copyright 2022, Elsevier. **b** and **c** Initial particle delocalization of PtNi nanoparticles showing octahedral shape with strong faceted shape in the (111) plane and

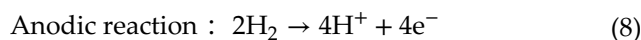
specific surface and three-dimensional morphologies at designated potentials. Vera et al. [80] employed an in situ electrochemical liquid cell integrated with scanning transmission electron microscopy (STEM) to analyze carbon corrosion and elucidate the degradation mechanisms of front-shaped Pt-Ni alloy nanoparticles supported on carbon substrates. Both the migration and detachment of Pt and Ni particles can result in a reduction of the ECSA, leading to decreased electrode activity and consequently a loss of power in the PEMFC. Additionally, carbon corrosion under high potential facilitates particle migration, as evidenced in STEM images of Pt-Ni nanoparticles before and after the test (Fig. 2b–c). It was observed that Pt-Ni nanoparticles, initially uniformly distributed on the (111) surfaces of carbon supports, agglomerated post-testing. These particles exhibited slight concave edges and cuts, indicating that these facets are relatively enriched in nickel, which erodes more rapidly during acid and electrochemical treatment, ultimately leaving a Pt-rich surface. Amirkoushyar et al. [81] used two imaging modes, bright-field (BF) STEM and high-angle annular dark-field (HAADF) STEM, to electronically analyze the Pt/C catalysts. BF STEM is utilized to detect lighter elements and primarily characterizes carbon, whereas HAADF STEM, being sensitive to the atomic number of elements, predominantly characterizes Pt. During the analysis of Pt/C catalysts, both sets of STEM images are captured simultaneously to gather complementary information. However, the original images often contain artifacts that result in blurriness. To mitigate these artifacts and enhance the characterization of carbon and platinum, a model-based iterative reconstruction with adaptive

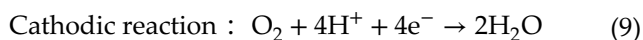
delocalization after 40 electrochemical voltammetry cycles with curved face shape and aggregation of Pt particles. Reproduced with permission from reference [80]. Copyright 2019. Royal Society of Chemistry.

regularization (MBIR-ARAR) method is proposed. This approach integrates an adaptive regularization step into the standard MBIR process. Two correction techniques are compared, whereby images of Pt and C are separately reconstructed in the X–Y and X–Z planes to eliminate streaks and artifacts. This methodology facilitates a clearer visualization of the distribution of Pt nanoparticles and pores within the carbon supports, providing crucial insights into the kinetic dynamics of the Pt catalysts.

Support materials for Pt-based catalysts

The catalyst and membrane-electrode assembly (MEA) constitute the core components of PEMFCs. The catalyst layer (CL) comprises the catalyst, catalyst support, and electrolyte membrane [82, 83]. The microstructure of the CL governs the transport properties of electrons, protons, reactants, and products, which directly influence cell performance. Catalysts employed in these systems include Pt and Pt-based alloys, Pd and Pd-based alloys [84, 85], non-precious metal catalysts such as Fe and Co, and non-metallic catalysts [86, 87]. Electrolyte membranes facilitate proton conduction from the anode to the cathode while also serving as barriers to electron transport. Within the CL, the catalyst support plays a pivotal role in hosting the reactions, forming a three-phase boundary (TPB) [85], where both the HOR and ORR transpire at the interfaces of the anode and cathode CL, respectively.





Catalyst supports are predominantly categorized into carbon-based and carbon-free types. Carbon-supported Pt is the most utilized variant, where the carbon support significantly influences the structural and performance characteristics of catalysts [88]. Carbon materials possess intrinsic properties such as porosity, a high surface area, and excellent electrical conductivity. These characteristics not only facilitate the uniform dispersion of the active metal but also provide ample space for electron conduction and gas diffusion, crucial for optimizing catalyst function.

Critically, the formation of coordination bonds between the d-orbitals of Pt and the p-orbitals of the carbon support facilitates direct metal-support interactions, which effectively lower the Fermi energy level. This reduction in Fermi energy enhances catalytic activity, thereby substantiating the premise that carbon materials are optimally suited as supports for catalysis [89]. Carbon support structures encompass a variety of forms including carbon black [90], mesoporous carbon [91], graphene [92], carbon nanotube(CNT) [93], carbon nanofiber (CNF) [94],

among others. These different carbon support structures significantly influence the ORR activity and durability of the catalyst layer [95]. Juan C et al. [96] investigated the effects of various carbon supports by loading PtNi alloy catalysts on CNTs and CNFs, producing PtNi/CNT and PtNi/CNF composites. Figure 3a displays the XRD patterns of unloaded PtNi nanoparticles alongside those loaded on CNTs and CNFs. Notably, the XRD patterns of the loaded PtNi nanoparticles exhibit an additional Bragg reflection at 25.71° , corresponding to the characteristic peak (002) of carbon materials used as supports. The ORR activities of the PtNi/CNT, PtNi/CNF, and Pt/C catalysts were evaluated using the RDE technique, recording half-wave potentials ($E_{1/2}$) of 0.89, 0.87 and 0.89 V vs RHE, as shown in Fig. 3b.

However, carbon supports are susceptible to inevitable corrosion issues that compromise their stability and longevity [97, 98]. The carbon corrosion process typically results in the production of CO_2 or CO , which diminishes the quantity of carbon remaining in the support. Notably, the electrochemical oxidation of carbon is observed to commence at a potential of 0.207 V.

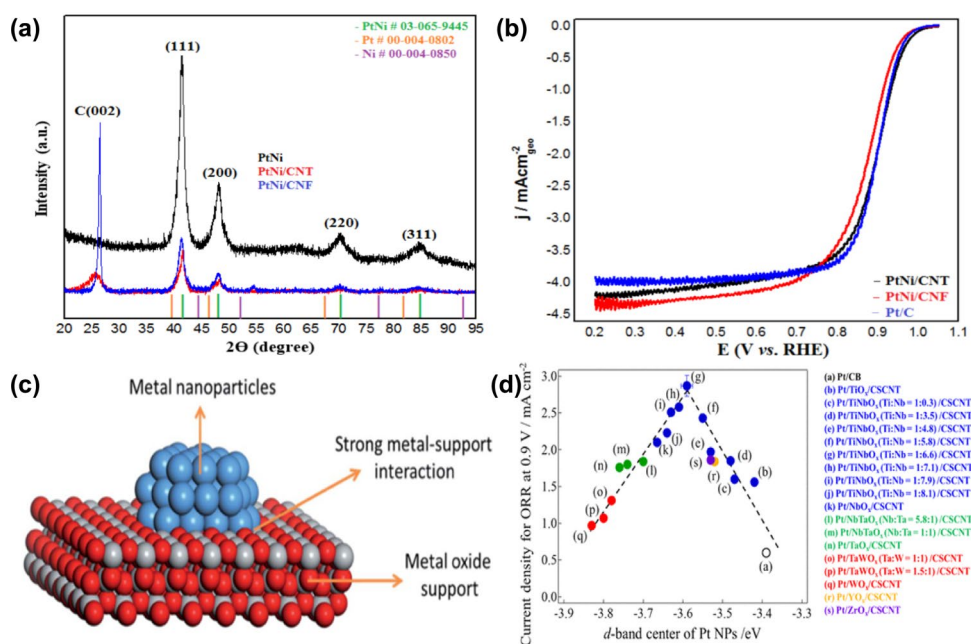
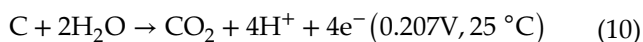
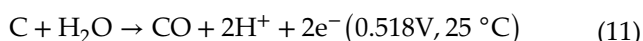


Figure 3 **a** XRD patterns of PtNi, PtNi/CNT and PtNi/CNF. ©2022, MDPI. **b** ORR polarisation curves of PtNi/CNT, PtNi/CNF and Pt/C catalysts in O_2 saturated 0.1 M HClO_4 solution. Reproduced with permission from reference [96] Copyright 2022, MDPI. **c** Schematic of strong metal-support interactions.

Reproduced with permission from [101]. Copyright 2020, Royal Society of Chemistry. **d** Variation of d-band center values of Pt loaded on different metal oxide supports. Reproduced with permission from [102]. Copyright 2021, American Chemical Society.



In practical applications, CL is integrated into a MEA, where the operational voltage exceeds the corrosion potential of the carbon support, rendering carbon corrosion an unavoidable phenomenon. Typically, the average output voltage of the MEA is greater than 0.6 V. During operation, the carbon support undergoes further oxidation, leading to the formation of CO. This reaction product, CO, induces structural modifications in the Pt nanoparticle catalysts, a detrimental effect known as CO poisoning.



Conversely, electrochemical induction facilitates the formation of oxygen functional groups on the carbon surface, precipitating the degradation of the carbon support. This degradation process contributes to the detachment of Pt nanoparticles and subsequent catalyst failure. The underlying mechanisms of this degradation include Ostwald ripening, particle agglomeration, and the dissolution and reprecipitation of Pt in the dissociative phase [99, 100]. Collectively, these phenomena result in a decrease in ECSA and diminished performance of the PEMFC.

The performance of carbon support can be enhanced through various strategies tailored to their specific properties. Key approaches include: (1) enhancing the durability of the CL by altering the carbon structure to minimize corrosion, thereby extending the operational lifespan of proton exchange membrane fuel cells (PEMFCs); and (2) increasing the intrinsic activity of the ORR by doping carbon supports with heteroatoms such as N, S, P, and B.

An alternative strategy involves employing non-carbon substrates, including nitrides [101], borides, mesoporous SiO₂, conducting polymers [103] and transition metal oxides (MO_x, M = Ti, Ta, Sn, W, Y, Zr, etc.) [104]. Among these, transition metal oxides are particularly noteworthy due to their strong resistance to chemical and electrochemical oxidation, significantly enhancing the durability and stability of catalysts. As shown in Fig. 3c, metal oxide supports and loaded metal nanoparticles experience robust metal-support interactions (SMSI), which markedly enhance catalytic activity. When NPs are supported on metal oxides, the supports donate electrons to the Pt NPs through SMSI effects, resulting in varied shifts in the d-band centers of Pt. These specific catalyst-support interactions

during the nucleation and growth of Pt NPs can be elucidated through density functional theory (DFT) analysis. The downward shift in the d-band centers of Pt atoms on the catalyst surface reduces the binding energy between Pt and oxygen-containing intermediates, thereby facilitating the desorption of reaction intermediates and modifying ORR activity. Fuma et al. [102] engineered Pt NPs on various metal oxides and manipulated the d-band center of Pt by adjusting the ratio of different metals. As shown in Fig. 3d, the ORR activity and the d-band center of Pt exhibit a “volcano” relationship. Initially, as the d-band center decreases, ORR activity increases, reaching a peak before subsequently declining. The peak ORR activity occurs when the d-band center is at -3.59 eV, with the optimal catalyst material being Pt/TiNbO_x (Ti/Nb = 1:6.6).

To optimize the utilization of metal oxides as catalyst supports, two primary strategies are employed: (1) doping with rare earth metals or additional transition metals to induce unique electronic effects, and (2) forming composites with carbon to enhance electronic conductivity. Among various oxides, TiO₂ stands out due to its exceptional corrosion resistance and relatively high electrical conductivity compared to other oxide materials. Consequently, this paper will also discuss advancements in employing TiO₂ as a support in catalyst development, in addition to carbon-based materials (Fig. 4).

Mesoporous carbon (MC)

Mesoporous carbon offers significant advantages, including a high specific surface area and high porosity. These properties not only effectively inhibit the aggregation of Pt-based nanoparticles (NPs) but also reduce the Pt loading, thereby lowering the fuel cell cost. New structures of mesoporous carbon, such as ordered mesoporous carbon (OMC), have been developed to enhance performance and durability at low Pt loadings [105]. The use of OMCs has been extensively investigated in recent years, focusing on improving the binding of Pt-based intermetallic NPs to mesoporous carbon to increase fuel cell durability. To enhance the activity and durability of Pt-based catalysts for ORR, Yi Yang et al. [106] prepared PtCo/OMC catalysts using solvent evaporation-induced self-assembly (EISA) and current substitution, with OMC serving as the carbon support. The orderly arrangement of OMC pores allows for uniform distribution of PtCo NPs. As a result, PtCo/OMC exhibited relatively high

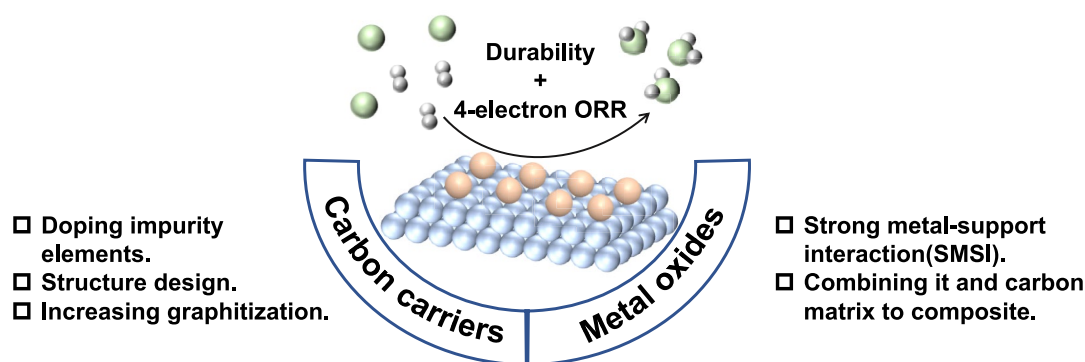


Figure 4 Pathways to improved performance of Pt-based catalyst support.

electrocatalytic activity and stability due to its ordered mesoporous structure. A control group loaded on Vulcan@XC-72 is also established. In electrochemical tests, PtCo/OMC exhibited a high ECSA value of 88.56 m²/g and an ECSA retention of 77.5% after 5000 CV cycles, which is higher than that of PtCo/XC-72 (83.41 m²/g and 65.5%). The Raman spectra shows that the degree of disorder in the carbon structure is usually analyzed by the intensity ratio I_D/I_G . The intensity of the d and g bands of PtCo/OMC is much higher than that of PtCo/XC-72, suggesting the presence of more sp² and sp³ groups. On the other hand, high d-band values indicate that OMCs are rich in defective structures, which can provide more active ORR sites. Yifei et al. [107] prepared PtCo@sOMC-T-1/x catalysts using OMC as the carbon support, where T represents the annealing temperature and x denotes the Co content. OMC aids in ordering the intermetallic compound atoms. By tuning the process flow and elemental composition, it is found that PtCo@sOMC-900-1/3 has the best kinetic activity at 0.95V. It has a relatively low d-band center, and the $E_{1/2}$ and ORR activities are significantly higher than those of other synthetic materials.

In addition to optimizing the MC synthesis process, modifying carbon supports with dopant elements such as N, S and P can tune the electronic structure and benefit the metal–carbon interaction. Yinlei et al. [108] used ammonium persulfate (APS) as a modifier to convert ordered mesoporous carbon (MC) CMK-3 into modified ordered mesoporous carbon (MMC), and loaded Pt₃Cu onto the two sets of carbon supports to obtain Pt₃Cu/MC and Pt₃Cu/MMC. The Raman spectra of these carbon support reveals that the intensity of both peaks is higher for MMC than that of MC, and the I_D/I_G ratio of MMC is greater

than that of MC, indicating improved graphitization of MC. The highly graphitized carbon structure features enhanced electronic conductivity and corrosion resistance. LSV curves of Pt₃Cu/MMC, Pt₃Cu/MC and JM-Pt/C catalysts with half-wave potentials are in the order of Pt₃Cu/MMC (0.928 V) > Pt₃Cu/MC (0.907 V) > JM-Pt/C (0.870 V). Compared to commercial Pt/C catalysts and undoped modified MC, the electrochemical performance of MMC is improved. As a result, the Pt₃Cu/MMC catalyst exhibited a mass activity of 0.58 A/mg_{Pt}, which is 4.8 times higher than that of JM Pt/C (0.12 A/mg_{Pt}).

The successful application of OMC in catalysis strongly validates the effectiveness of using mesoporous carbon as support materials. However, the issue of carbon corrosion persists, necessitating the development of innovative strategies to address this challenge.

Graphene

To decrease the use of platinum group metals (PGMs) and boost catalyst durability, researchers are investigating the use of graphene as a support for Pt-based catalysts. Graphene effectively leverages its strong adsorption capacity for reactants via interactions with π -electrons, making it an excellent catalyst support [109, 110]. Graphene is added to electrolytes to enhance proton conductivity and increase the output power of the fuel cells. Zipeng et al. [111] reported a graphene nanopocket design in which PtCo is encapsulated in a non-contact graphene nanopocket to form a core–shell structure to obtain a PtCo@Gnp catalyst (Fig. 5a). As shown in Fig. 5b–c, in the MEA test, the MA and MA residuals

at the Beginning of Life (BOL) and End of Test (EOT) of PtCo@Gnp with a cathode loading of $0.06 \text{ mg}_{\text{PGM}}/\text{cm}^2$ exceeded the U.S. Department of Energy (DOE) targets and were much larger than those of commercial Pt/C catalysts and c-PtCo/C. This suggests that the unique structure effectively inhibits catalyst aggregation and slows the processes of oxidative dissolution, diffusion, and Ostwald ripening during electrochemical reactions. Such characteristics are

anticipated to enhance fuel cell durability even at ultra-low PGM loadings.

Numerous types of graphene-based materials, known for their high stability and electrocatalytic capabilities, are being explored as carbon supports [112, 113]. Recent studies on the properties of graphene-based materials have revealed that metal-free doped graphene-based catalysts exhibit outstanding ORR catalytic activity. This advantageously

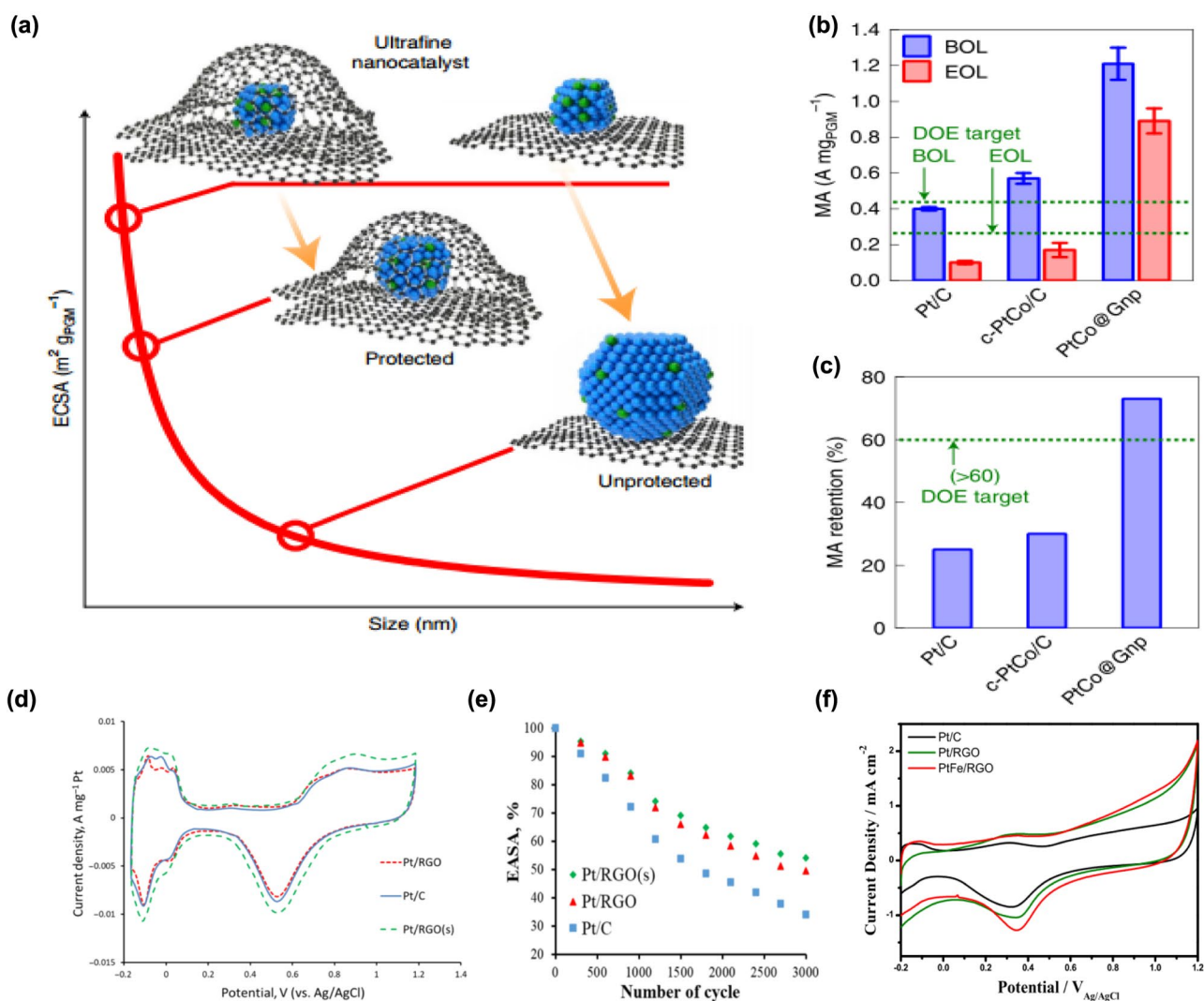


Figure 5 a Schematic representation of ultrafine nanocatalysts in graphene pockets and their effect on ECSA retention after ADT. b–c MA test plot and MA retention after 30,000 ADTs in Pt/C, c-PtCo/C and PtCo@Gnp, in N_2 -saturated 0.1M HClO_4 solution at a scan rate of 20 mV/s [111]. Reproduced with permission from reference [111]. Copyright 2022, Nature. d CV plots of Pt/C, Pt/RGO, and Pt/RGO(s) in N_2 -saturated 1 M

H_2SO_4 solution with a scan rate of 20 mV/s. e Catalyst ECSA retention after AST cycling. Reproduced with permission from reference [117]. Copyright 2021, MDPI. f CV plots of PtFe/RGO, Pt/RGO and Pt/C in N_2 -saturated 0.5 M H_2SO_4 solution with a scan rate of 50 mV/s. Reproduced with permission from reference [118]. Copyright 2022, MDPI.

circumvents the issues associated with the dissolution of metal nanoparticles, thereby potentially reducing costs and enhancing catalyst durability [114, 115]. Graphene-based materials, such as graphene oxide (GO), reduced graphene oxide (RGO), and heteroatom-doped graphene, have also been utilized as carbon supports and have demonstrated superior properties [116]. The efficiency of platinum utilization in catalysts supported on graphene-based substrates is strongly influenced by the synthesis process and the type of precursor used. These factors have been the subject of intensive investigation by researchers. Irina V et al. [117] synthesized Pt-based catalysts loaded with RGO, Pt/RGO and Pt/RGO(s) using a conventional two-step polyol process and a modified polyol process, and compared them with the Pt/carbon black Vulcan XC-72© Pt/C catalyst. Figure 5d shows the CV plots. The ECSAs for Pt/C, Pt/RGO and Pt/RGO(s) calculated from Eq. 4 are approximately 54, 48 and 60 $\text{m}^2/\text{g}_{\text{Pt}}$, respectively. As shown in Fig. 5e, after 3000 accelerated stress test (AST) cycles, the ECSA residual rates of Pt/C, Pt/RGO and Pt/RGO(s) are 34, 49.5 and 53.9%, respectively, indicating that the optimized synthesis process transformed RGO into a more ordered sp^2 graphite structure, which well suppressed particle agglomeration and dissolution. Bathinapatla et al. [118] prepared bimetallic PtFe NPs loaded on RGO by a simple surfactant-free chemical reduction method and compared them with Pt and commercial Pt/C catalysts loaded on RGO. As shown in Fig. 5f and g, the calculated ECSAs of Pt/C, Pt/RGO and PtFe/RGO are 33.52, 37.35 and 39.89 m^2/g , respectively. The $E_{1/2}$ of the ORR polarization curves are 0.336, 0.352 and 0.503 V. The enhancement of ORR activity was attributed to the modification of the carbon supports. Furthermore, doping Fe into the Pt lattice significantly altered the electronic structure of Pt. Employing graphene-based materials in conjunction with bimetals substantially enhanced the durability of the catalysts.

Carbon nanotube (CNT)

Carbon nanotubes, one-dimensional tubular materials composed of sp^2 -hybridized carbon atoms, are extensively utilized in various applications. They are widely used as catalyst support materials for ORR in acidic media, PEM fillers [119] and metal-free catalysts [120]. In carbon nanomaterials, CNTs feature hollow nanostructures. Their high surface-to-volume ratio and the low density within the hollow interiors are

advantageous for exposing catalytic active sites and facilitating efficient charge transfer. These properties lead to significant enhancement in electrocatalytic activity. CNTs can be categorized into single-walled carbon nanotubes (SWCNTs) and multi-walled carbon nanotubes (MWCNTs). SWCNTs consist of a single layer of graphene seamlessly wrapped in a cylindrical tube, whereas MWCNTs consist of a series of SWCNTs of different diameters. MWCNTs exhibit relatively lower conductivity and increased surface defects. The presence of more surface defects enhances their capacity to immobilize nanoparticles and prevent their aggregation, thereby positioning MWCNTs as highly promising candidates for catalyst applications [121]. Yu Yao et al. [122] investigated the effect of sp^2 carbon material type on catalyst ORR performance using one-pot ionic liquid pyrolysis with two ionic liquids, 1-butyl-3-methylimidazolium bis(trifluoromethanesulfonyl)amide ($[\text{C}_4\text{mim}][\text{Tf}_2\text{N}]$) and N,N,N-trimethyl-N-propylammonium bis(trifluoromethanesulfonyl)amide ($[\text{N}_{1,1,1,3}][\text{Tf}_2\text{N}]$), respectively. Both Pt/MWCNT catalysts are prepared by loading Pt NPs onto MWCNTs, and the effects of the two ionic liquids on the size of the Pt NPs are shown in Fig. 6a. The performances of the two Pt/MWCNT catalysts are compared with commercially available Pt/C catalysts. After 15,000 potential cycle durability tests, the two Pt/MWCNT catalysts achieved ECSA retention of 75.1% and 92.8% respectively, both higher than Pt-C (71.1%). In terms of mass activity, both catalysts demonstrated greater durability than the commercially available Pt/C catalyst. The results reveal that the Pt/MWCNT samples synthesized using ionic liquids exhibit high retention rates. This finding underscores the potential of ionic liquids as a method for the synthesis of ORR electrocatalysts that are both highly durable and stable.

MWCNTs possess numerous defect sites predominantly located at the edges, ends, and sidewalls of the nanotubes, making them viable candidates for enhancing the electrocatalytic activity of ORR. Leveraging this characteristic, MWCNTs can be doped with impurity elements. These impurities are introduced at the existing defect sites, creating new defects that alter the electronic structure of the MWCNTs. Such modifications not only provide active sites for various electrochemical reactions but also improve the conductivity and overall electrochemical activity of MWCNTs [123, 124]. Phiralang et al. [125] prepared N-doped multi-walled carbon nanotubes, Mel-NCNT and Hex-NCNT,

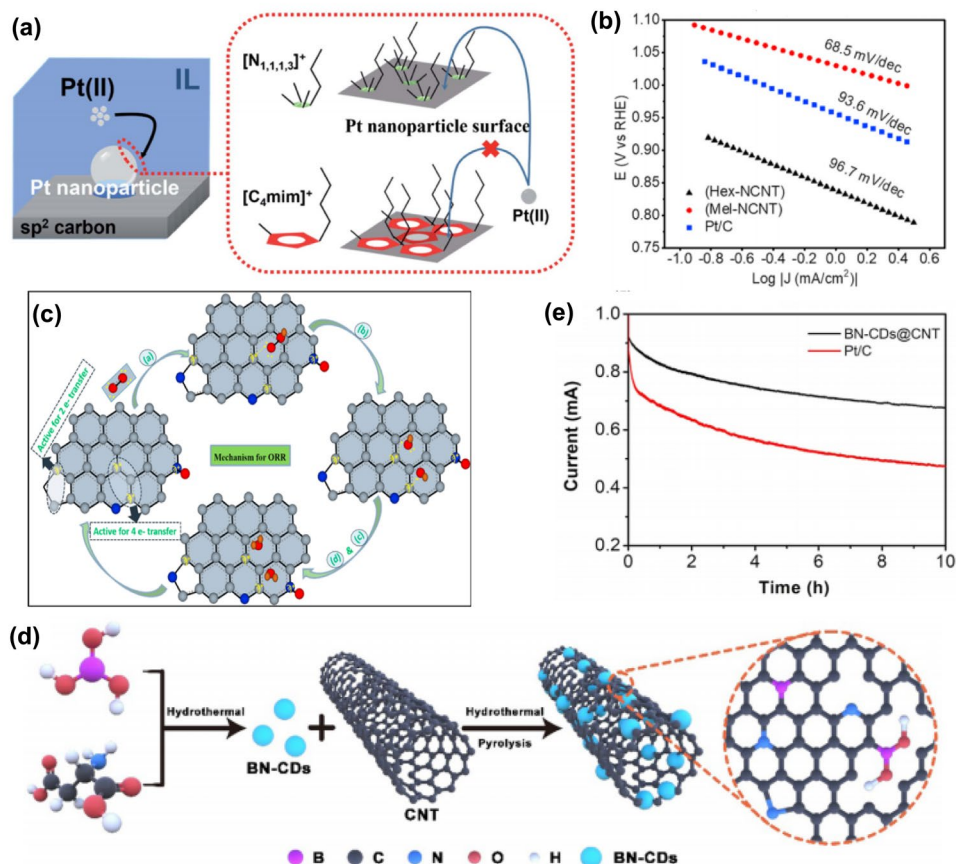


Figure 6 **a** Schematic representation of the effect of organic cationic substances in $[N_{1,1,1,3}][Tf_2N]$ and $[C_4mim][Tf_2N]$ on the size of Pt NPs. Reproduced with permission from reference [122]. Copyright 2022, Royal Society of Chemistry. **b** Tafel plots of the ORR of Hex-NCNT, Mel-NCNT and Pt/C in 0.1 M KOH alkaline solution under O_2 saturation. **c** Schematic representation of the mechanism of the $4e^-$ -ORR pathway for the action

using melamine and tetrazolium hexamine as the nitrogen source, respectively. Mel-NCNT ($I_A/I_D = 0.99$) showed a higher d-band intensity than Hex-NCNT ($I_A/I_D = 0.95$). As shown in Fig. 6b, the Tafel slope of Mel-NCNT is obviously smaller than that of Pt/C and Hex-NCNT, which indicates that Mel-NCNT has excellent ORR activity and illustrates the good doping effect of melamine as a nitrogen source. It is also found that the nitrogen-doped site has the selectivity of the $4e^-$ -ORR pathway, as shown in Fig. 6c, but the exact principle remains to be analyzed. Yanfei et al. [126] on the other hand, synthesized B-N co-doped multi-walled carbon nanotubes by hydrothermal reaction and calcination to produce BN-CDs@CNT, as shown in Fig. 6d. Timed current measurements are carried out in an alkaline

of nitrogen-doped pyridine-N and oxidized-N sites. Reproduced with permission from reference [125]. Copyright 2021, Elsevier. **d** Schematic representation of the synthesis of BN-CDs@CNT. **e** Long-term stability test of BN-CDs@CNT and Pt/C catalysts at 0.7 V (vs RHE). Reproduced with permission from reference [126]. Copyright 2021, Elsevier.

solution of 0.1 M KOH at a constant potential of 0.7 V for 10 h. As shown in Fig. 6e, after 10 h of testing, the current density of BN-CDs@CNT is 76%, while that of Pt/C decreased to 52%. The results indicated that the BN-CDs@CNT catalysts possessed excellent ORR performance and cycling stability. According to DFT calculations, nitrogen and boron doping in CNTs can enhance the reactivity of platinum on the CNT surface. It is anticipated that carbon catalysts doped with multiple elements will demonstrate a synergistic effect superior to that of singly doped carbon catalysts. Specifically, when loaded with platinum, these multi-element doped catalysts are expected to achieve enhanced ORR performance with reduced platinum loading.

MWCNTs are extensively utilized across various fields, particularly as catalyst supports in fuel cells. Attaching NPs to the smooth and chemically inert surfaces of sp^2 -bonded carbon materials poses significant challenges. Furthermore, the wrapping layers of CNTs can experience considerable corrosion during fuel cell operation. By doping with impurity elements, these issues can be effectively mitigated, enhancing the corrosion resistance of MWCNTs and thereby improving the longevity and performance of fuel cells.

Carbon nanofiber (CNF)

Carbon nanofibers serve as catalyst support, capitalizing on their unique porous structure to enhance the transport of gases, liquids, and electrons. Furthermore, the carbon atoms located at the edges of CNFs amplify the exposure of active sites for the ORR. In fuel cell applications, it can also be added to Nafion nanocomposite membranes as a filler to increase the power density and durability of fuel cells [127]. Electrostatic spinning, recognized as one of the most effective methods for producing nanofibrous filaments [128], results in electrospun carbon fibers that possess a highly graphitized carbon structure. Due to its high electrical conductivity and corrosion resistance, carbon nanofibers are acknowledged as a highly active and durable catalyst support. The loaded catalysts exhibit enhanced electrocatalytic activity and more efficient catalyst utilization. Electrostatic spinning has emerged as the predominant preparation method for PEMFC electrodes. Sunki et al. [129] improved the process of electrostatic spinning technology and applied two different graphitization methods—thermal graphitization and catalytic graphitization—to CNF. Fibrous carbon materials are prepared by electrostatic spinning technology, thermal graphitization and catalytic graphitization. Pt catalysts are synthesized by polyol method on three different types of fibrous carbon supports—ordinary CNF support, thermo-graphitized CNF support (GCF-HT), and catalytic graphitized CNF support (GCF-(Co)). As shown in Fig. 7a-f, the Pt NPs are uniformly distributed in GCF-(Co) when loaded onto it, which proved that GCF-(Co) has a highly porous structure and well controls the particle size distribution of Pt, with the particle size mostly concentrated at 3–4 nm. After the AST test, as shown in Fig. 7g-h, the corrosion resistance of the carbon is significantly improved compared to the commercial sample Pt/C-TKK, and the decrease in $E_{1/2}$ is very small, indicating

that the catalyst has good electrocatalytic activity. The improvement of the CNF synthesis process can increase the degree of graphitization and thus increase the service life of the fuel cell.

As carbon support, CNFs are susceptible to carbon corrosion. Enhancing the degree of graphitization in carbon supports can effectively mitigate this issue. As a result, highly graphitized CNFs have been the focus of extensive research and application. Furthermore, the incorporation of dopant atoms into carbon nanomaterials not only reduces carbon corrosion but also improves the activity and cycling stability [130, 131]. This enhancement is attributed to the altered electronic structure of carbon nanomaterials. In recent years, extensive research has been undertaken to investigate these factors with the goal of achieving improved performance. Srinu et al. [132] prepared N-F co-doped GNFs supports, GNFs-NFs, and then loaded Pt NPs onto GNFs-NFs using a modified ethylene glycol (EG) reduction synthesis method. In order to investigate the effect of the shape of the linear arrangement of GNFs—(lamellar (L), antler (A) and herringbone (H)) on the ORR performance, they synthesized L-Pt, A-Pt, H-Pt, L-NF-Pt, A-NF-Pt and H-NF-Pt cathode catalysts. As shown in TEM images (Fig. 7i-n), the GNFs-NF supports resulted in fine particle size and concentrated size distribution of Pt NPs, with the majority falling within 3 ~ 4 nm, indicating that the N-F co-doping makes the particles smaller in size and more homogeneously dispersed. Figure 7o shows two indicators, mass activity (MA) and specific activity (SA), of the ORR activity of the catalysts. The MA and SA of L-NF-Pt, A-NF-Pt and H-NF-Pt are significantly higher than those of L-Pt, A-Pt and H-Pt, but significantly lower compared to the commercial Pt/C catalysts. The ECSA of L-Pt, A-Pt, H-Pt, L-NF-Pt, A-NF-Pt, H-NF-Pt and Pt/C measured by the RDE technique are 113, 119, 123, 69, 70, 72 and 87 m^2/g respectively. As shown in Fig. 7p, after the AST test, it is found that the loss of ECSA of H-NF-Pt is minimized and the synergistic effect produced by the co-doping of N and F resulted in higher electrochemical performance and durability of L-NF-Pt, A-NF-Pt and H-NF-Pt catalysts.

Currently, the primary focus with CNFs revolves around achieving stable graphitic structures. By refining the synthesis processes, the desired structures can be obtained, leading to a significant improvement in catalyst corrosion resistance. Highly graphitized GNFs are extensively researched as a result. Researchers have found that different

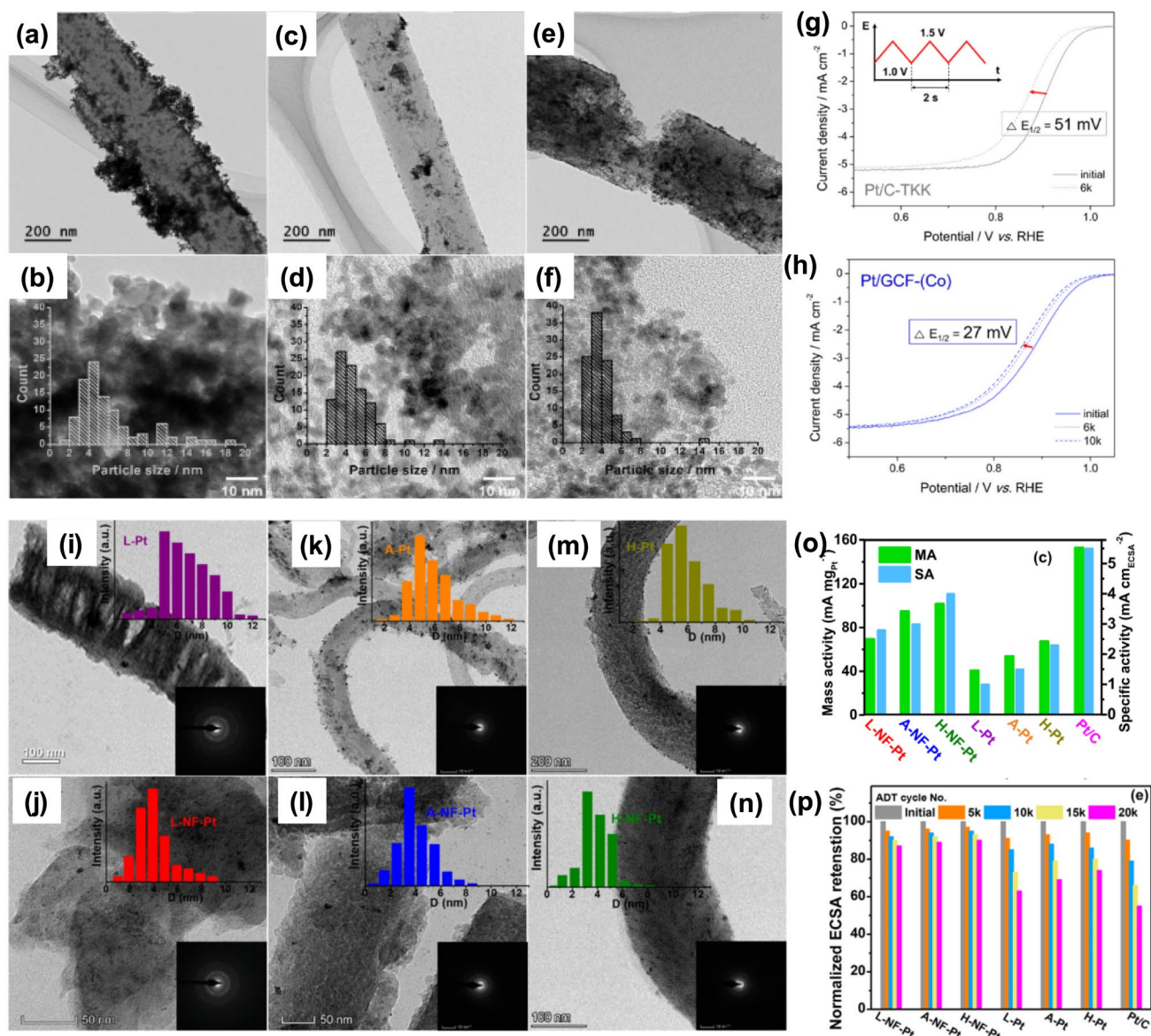


Figure 7 HR-TEM images of **a** Pt/CNF, **c** Pt/GCF-HT and **e** Pt/GCF-(Co). **b**, **d** and **f** Particle size distributions of loaded Pt NPs. **g–h** Changes in $E_{1/2}$ of the commercial samples Pt/C-TKK and Pt/GCF-(Co) after 6,000 and 10,000 AST cycles at 25°C, measured in O_2 -saturated 0.1 M $HClO_4$ with LSV and a scan rate of 5 mV/s. Reproduced with permission from reference [129]. Copyright 2020, Elsevier. TEM images of **i** L-Pt, **k** A-Pt, **m**

H-Pt, **j** L-NF-Pt, **l** A-NF-Pt, and **n** H-NF-Pt, along with the corresponding SAED patterns and particle size distributions of the samples. **o** Mass activity (MA) and specific activity (SA) values of catalysts. **p** Changes in ECSA values of catalysts during ADT cycling. Reproduced with permission from reference [132]. Copyright 2022, Elsevier.

types of GNF structures have varying impacts on reactions in fuel cells. Hexagonal GNF as an ORR catalyst warrants further in-depth investigation.

Carbon black (CB)

Carbon black as a carbon support material for catalysts is cost-effective and mechanically flexible. However, unlike other carbon support materials such as mesoporous carbon, graphene, carbon nanotubes, and carbon nanofibers, CB has a low degree of graphitization. The level of graphitization reflects the number of defects in the carbon support. Typically, carbon corrosion begins at defective sites, with the degree of graphitization determining the resistance or sensitivity of the carbon support material to carbon corrosion. To enhance the graphitization degree of carbon black, researchers have combined carbon black with other carbon materials to form unique hybrid support structures, aiming to improve durability while maintaining the performance of Pt-based catalysts. Zhou T et al. [133] mixed prepared porous carbon nanofibers (PCNFs) with different mass ratios (20%, 30%, 40% and 50%) of CB to produce hybrid supports for Pt nanoparticles. The Pt NPs are then loaded onto the composite support by the glycol reduction method, and the resulting Pt/(PCNF + CB) is used as a cathodic electrocatalyst. As shown in Fig. 8a–h, with increasing CB content, the PCNFs and CB are evenly distributed to form carbon composite supports. Analyzed by the LSV test, as shown in Fig. 8i, the $E_{1/2}$ of Pt/(PCNF + CB)-40% is 0.799 V, which is 25 mV higher than that of Pt/C (0.774 V), the commercial Pt/C sample. It is suggested that the superior ORR performance of the former is attributed to the porous structure of PCNFs and CB stacking, which enhances oxygen transfer and the oxygen reduction rate. Furthermore, accelerated durability tests (ADT) conducted on these catalysts demonstrate that the durability of those utilizing composite supports markedly exceeds that of commercial samples. This enhanced durability is likely due to their improved graphitization.

To enhance the stability of carbon composite performance, the electronic structure is also modified through the incorporation of impurity elements. Zhaoqi et al. [134] mixed electrochemically exfoliated graphene oxide (EGO) containing $-NH_2$ groups with CB to form a catalyst support-NrEGO-CB. The strong electron donor behavior of N enhances p-bonding and further improves ORR activity and catalyst durability.

As shown in Fig. 8j, NrEGO is prepared by a hydrothermal method, EGO is doped and reduced by nitrogen doping, and Pt is loaded onto the support by polyol reduction to form a Pt/NrEGOx-CBy catalyst. The ORR activity is analyzed by LSV test and as shown in Fig. 8k, the onset potential of Pt/NrEGO₃-CB₂ is 0.861 V, which is slightly higher than that of the commercial samples Pt/C (0.824 V) and Pt/NrEGO₂-CB₃ (0.819 V). As the amount of NrEGO flakes increased, the onset voltage gradually increased, indicating that the presence of N favors the initiation of the reaction. In addition, the electron transfer number of the N-doped hybridized support catalyst increased from 3.8 to 4.2 with an increase in the amount of NrEGO, indicating that the 4e reaction pathway with water as the product is effectively utilized to fully exploit the performance of the fuel cell. As shown in Fig. 8l, the Tafel slope of Pt/NrEGO₂-CB₃ is 67 mV/dec, which is much lower than that of the commercial Pt/C sample. Therefore, in terms of durability, the attenuation of the Pt/NrEGO₂-CB₃ MEA at 0.80 A/cm² after 30 k times of AST test is only 10 mV, while the attenuation of the Pt/C MEA at 0.80 A/cm² is 92 mV, indicating the high corrosion resistance of the composite carbon supports containing N.

Due to the low degree of graphitization, CB is susceptible to carbon corrosion. Combining CB with other carbon materials to form composite supports exploits synergistic effects among materials, enhancing both ORR activity and corrosion resistance—an effective strategy. To fully capitalize on the advantages of CB, it is essential to conduct research into material properties and preparation techniques that increase the binding strength between Pt NPs and CB, as well as enhance its graphitization level.

Metal oxide (TiO₂)

Metal oxides, unlike carbon, can serve as catalyst supports, effectively preventing carbon corrosion while exhibiting extremely high CO tolerance and stability. These properties result in lower onset potentials and higher current densities during electrochemical tests, thereby facilitating optimal ORR performance [135, 136]. Titanium dioxide (TiO₂) is renowned for its robust stability, exceptional photocatalytic properties, and non-toxic nature, making it a popular choice in diverse applications, from paints and sunscreens to pollutant degradation [137, 138]. Despite its advantages, TiO₂'s effectiveness is limited by its reliance

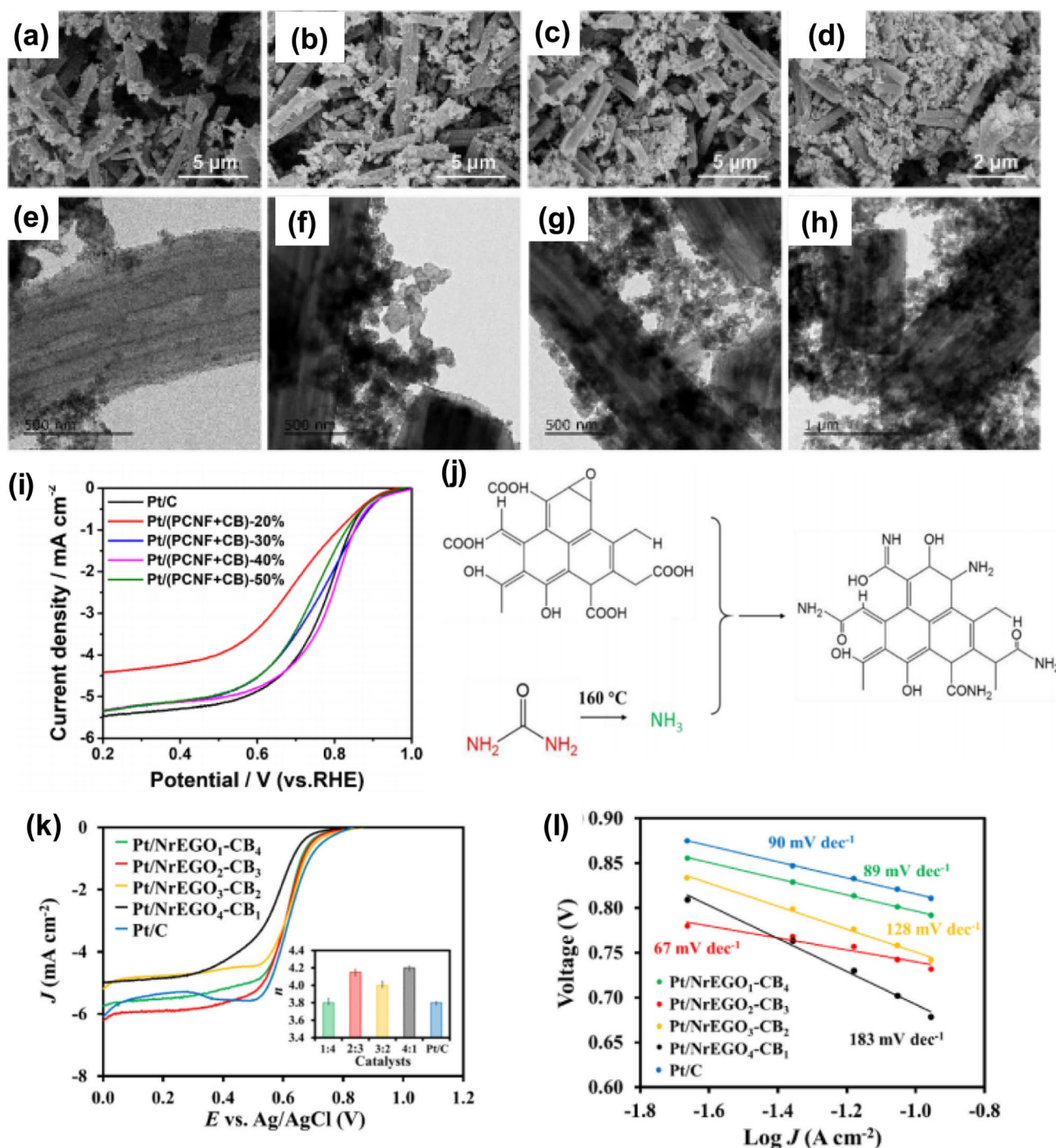


Figure 8 SEM image of the catalyst: **a** Pt/(PCNF+CB)-20%; **b** Pt/(PCNF+CB)-30%; **c** Pt/(PCNF+CB)-40%; **d** Pt/(PCNF+CB)-50%. TEM image of the catalyst: **(e)** Pt/(PCNF+CB)-20%; **(f)** Pt/(PCNF+CB)-30%; **(g)** Pt/(PCNF+CB)-40%; **(h)** Pt/(PCNF+CB)-50%. **i** LSV polarization curves in O_2 -saturated 0.5 M H_2SO_4 at a scan rate of 5 mV/s Reproduced with permission from reference [133]. Copyright 2022, MDPI. **j** Schematic representation of the preparation of electrochemi-

cally exfoliated graphene oxide (EGO) to nitrogen-doped reduced EGO (NrEGO). **k** LSV measures ORR activity and electron transfer number for all electrocatalysts with scanning from 1.0 to 0.0 V with a scan rate of 20 mV s^{-1} under O_2 saturated 0.5 M H_2SO_4 solution. **(l)** Tafel slopes for Pt/NrEGO_x-CB_y and Pt/C. Reproduced with permission from reference [134]. Copyright 2022, Elsevier.

on UV light, due to its wide bandgap, and the rapid recombination of photogenerated electron–hole pairs. For ORR, TiO_2 is explored for its potential to enhance the durability and activity of catalysts, particularly when used as a support material that can improve the dispersal and stability of active catalytic sites [139]. TiO_2 is extensively utilized in multiphase catalysis and has been explored as a catalyst support for fuel cells owing to its high stability in acidic and aqueous environments. Researchers have introduced rare metals into the TiO_2 lattice, which protects the doped metals from dissolution. This integration enhances conductivity and durability by forming a unique electronic structure, thus improving the overall efficiency of the catalyst [140]. To investigate the role of Pt–Mo bimetallic system in PEMFC, D. Diczhazi et al. [141] prepared $\text{Ti}_{1-x}\text{Mo}_x\text{O}_2$ -C composite supports by doping Mo into TiO_2 lattice using sol–gel method and mixing it with activated carbon. This new support for Pt-based catalysts has good stability and CO tolerance, and good SMSI when Ti:Mo = 4:1. Irina et al. [142] studied this in detail and prepared $\text{Ti}_{0.8}\text{Mo}_{0.2}\text{O}_2$ -C composite supports by mixing commercial (BP: Black Pearls 2000) with functionalized (FC) carbon materials loaded with 20 wt% and 75 wt% Pt using the glycol reduction precipitation method to obtain samples Pt/25BP, Pt/75BP, Pt/25FC-4 and Pt/75FC-4, respectively. As shown in Fig. 9a–b, the electrochemical stability of the catalyst is tested for 500 polarization cycles, and the ECSA is calculated from the capacitive current generated by charging the double layer of CV. The ECSA loss was recorded at 9.1% for Pt/25BP and 8.5% for Pt/75FC-4. Notably, the ECSA of Pt/25BP was higher than that of Pt/75FC-4, indicating that less Pt is needed for enhanced CO tolerance. Consequently, Pt/25BP demonstrates promising application prospects.

Enhancements in the electrical conductivity and electrocatalytic activity of ORR can be achieved by developing TiO_2 -activated carbon composite materials, where the activated carbon is required to be highly graphitized. A homogeneous dispersion of Pt NPs on metal oxide supports increases the ECSA and thus the utilization of Pt. Jian Kong et al. [143] prepared TiO_2 @CNT supports by sol–gel process combined with annealing process and anchored Pt NPs around TiO_2 nanoparticles by photodeposition technology, as shown in Fig. 9c. Figure 9d–e shows the HRTEM images of the synthesized Pt/ TiO_2 @CNT. Ultrafine Pt NPs with a lattice spacing of 0.227 nm are deposited around TiO_2 nanoparticles to form a

unique Pt- TiO_2 -CNT triple structure which has good properties. As shown in Fig. 9f, 10,000 cycles of ADT are used to test the durability of the supports. It was found that Pt/ TiO_2 @CNT has excellent ORR stability compared with the commercial sample Pt/C. After ADT, the ECSA of Pt/ TiO_2 @CNT and Pt/C decreased by 5.7% and 32.6% respectively. Chanmi et al. [144] used a hydrothermal method to prepare an NG- TiO_2 composite consisting of N-doped graphene and N-doped TiO_2 as a Pt-based catalyst support. Pt/NG- TiO_2 was compared with Pt/ TiO_2 , Pt/G- TiO_2 , Pt/NG- TiO_2 , and Pt/C catalysts. The initial $E_{1/2}$ of Pt/NG- TiO_2 , Pt/ TiO_2 , Pt/G- TiO_2 and Pt/NG- TiO_2 are 0.868 V, 0.843 V, 0.855 V and 0.85 V respectively. After 20,000 ADT cycles, the $E_{1/2}$ is 0.865 V, 0.831 V, 0.837 V and 0.81 V respectively. The $E_{1/2}$ loss of Pt/NG- TiO_2 is only 3 mV. The initial mass activity of Pt/NG- TiO_2 is 28.52 A/g_{Pt} and only 17.8% is lost after 20,000 ADT cycles. It is shown that Pt-based catalysts using N-doped activated carbon–metal oxide composite support have high durability and apparent stability.

Utilizing metal oxides as catalyst supports not only mitigates the issue of carbon corrosion but also allows for the adjustment of the d-band center of Pt in accordance with the SMSI principle, enhancing the catalytic activity for the ORR. However, incorporating metal oxides tends to exacerbate metal segregation. During continuous cyclic operations, Pt and other metal nanoparticles may aggregate, and the absence of a uniformly dispersed structure can precipitate catalyst degradation. To address this limitation, further investigation into the catalyst's structure is essential to identify an optimal configuration. Ensuring a uniform distribution of metal particles throughout the process represents a crucial direction for developing highly active and stable ORR catalysts. The Pt/ TiO_2 anode catalysts prepared by Sang-Hoon et al. [145] showed good HOR selectivity, which was mainly due to the fact that O_2 could not be transported through TiO_2 , thus inhibiting ORR. In contrast, under hydrogen-rich conditions, the insulating TiO_2 layer was reduced to a conductive TiOOH layer, achieving HOR selectivity. Pt/ TiO_2 catalysts with HOR selectivity showed a threefold increase in durability in MEA compared to commercial Pt/C catalysts. Stühmeier et al. prepared a Pt/ TiO_x /C ($x \leq 2$) anode catalyst that successfully mitigated cathodic carbon corrosion. The Pt particles are encapsulated by a thin layer of TiO_x ($x \leq 2$) and an SMSI effect is formed between Pt and TiO_x , which

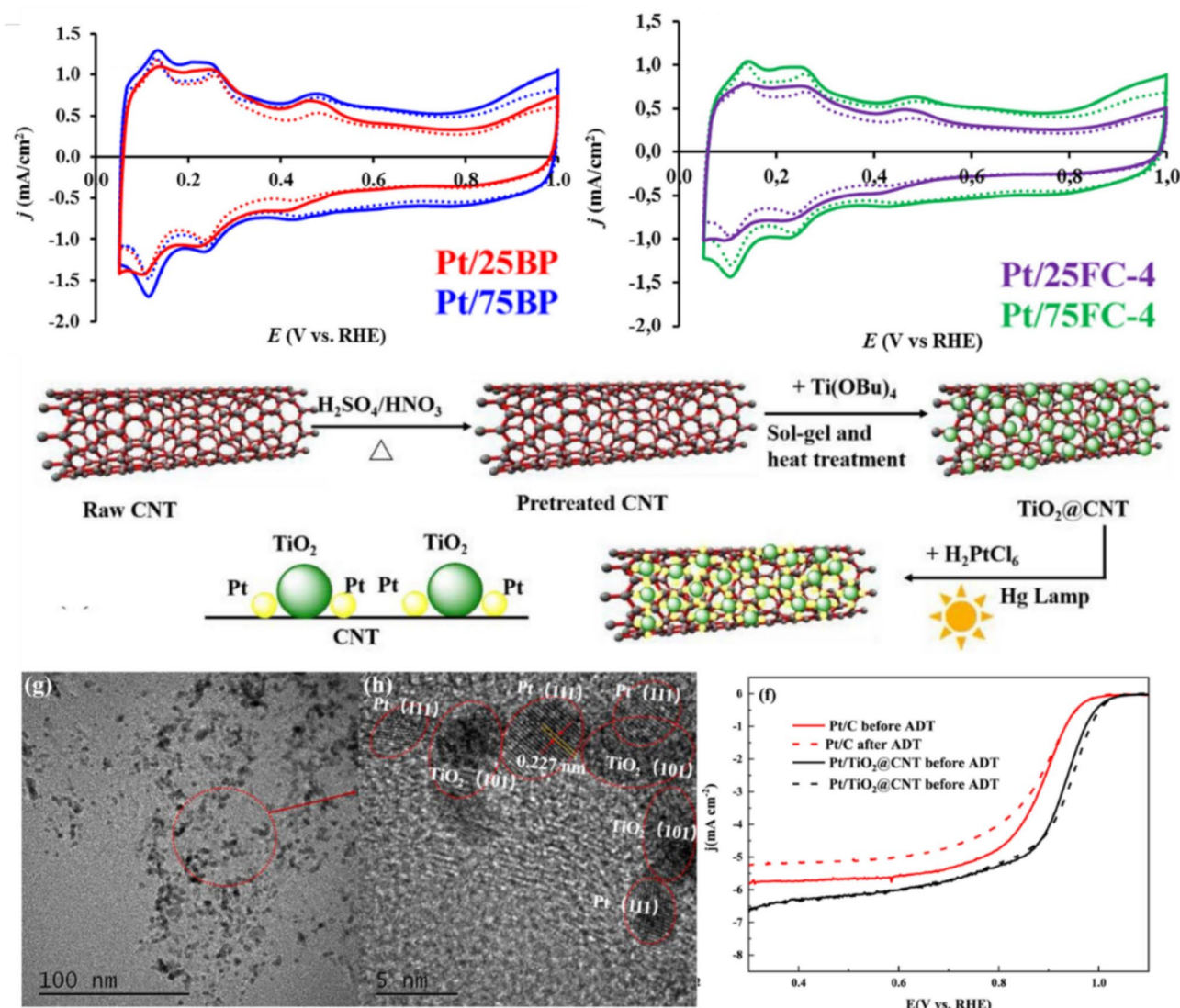


Figure 9 Effect of $\text{Ti}_{0.8}\text{Mo}_{0.2}\text{O}_2/\text{C}$ ratio on the electrochemical performance of catalysts in **a** BP and **b** FC-4 carbon composites, CV plots of electrocatalysts in 0.5 M H_2SO_4 solution with a scan rate of 100 mV/s before (solid line) and after 500 cycles (dashed line) of stability tests. Reproduced with permission from refer-

ence [142]. Copyright 2021, Elsevier. (c) schematic of $\text{Pt}/\text{TiO}_2/\text{CNT}$ synthesis. **d–e** HRTEM image of $\text{Pt}/\text{TiO}_2/\text{CNT}$. **f** LSV curves of $\text{Pt}/\text{TiO}_2/\text{CNT}$ and Pt/C before and after ADT in 0.1 M HClO_4 solution at 25 °C. Reproduced with permission from reference [143]. Copyright 2020, Elsevier.

reduced the ORR activity of the catalyst. The HOR selectivity of the $\text{Pt}/\text{TiO}_x/\text{C}$ catalyst is about 5 times higher than that of the conventional Pt/C catalyst. In the future, improving fuel cell durability by increasing anode HOR selectivity will be the mainstream of automotive PEMFC research.

Other materials such as graphitic carbon nitride ($\text{g-C}_3\text{N}_4$) was also explored for Pt-based catalysts [146, 147]. As a two-dimensional semiconducting polymer, $\text{g-C}_3\text{N}_4$ features a band gap of about 2.7 eV, which is

beneficial for facilitating charge separation. Its high thermal and chemical stability ensures durability under the harsh conditions typical of ORR processes. Moreover, the structure of $\text{g-C}_3\text{N}_4$ promotes efficient electron mobility, enhancing the overall electrocatalytic activity of Pt-based catalysts. These properties make $\text{g-C}_3\text{N}_4$ a promising support material in applications such as photocatalysis, water splitting, and sensors, and particularly valuable in enhancing the performance of Pt-based catalysts in oxygen reduction

reactions, crucial for advancing electrochemical energy storage technologies [148, 149].

To provide a clearer understanding of the various support materials available for Pt-based catalysts in oxygen reduction reactions, the following table summarizes their respective advantages, disadvantages, and potential applications (Table 1).

Discussion

Support materials are instrumental in enhancing overall catalyst performance. They enable the formation of complex catalyst structures, significantly reducing Pt usage by providing a high surface area for better dispersion of Pt nanoparticles. Additionally, support materials improve catalyst durability by stabilizing active sites and protecting them from degradation under harsh operating conditions. They also enhance ORR activity by optimizing the electronic and structural properties of the catalyst. Furthermore, advanced support materials improve mass transport and heat management within the catalyst layer, further boosting the efficiency and longevity of fuel cells [11]. Thus, developing novel support materials for Pt catalysts provides a promising solution to enhance catalyst performance.

Durability is a crucial characteristic when designing support materials for Pt-based catalysts, particularly in the context of ORR for fuel cells and other energy-related technologies [160–162]. To ensure these materials meet the rigorous demands of practical applications, it is essential to conduct comprehensive long-term stability tests. These evaluations help ascertain the material’s resilience to degradation over extended periods of use, a factor that directly influences the lifespan and efficiency of fuel cells [163]. Additionally, understanding the mechanisms behind the deterioration of support materials under various operational stresses such as fluctuating temperatures, chemical exposure, and mechanical stress provides invaluable insights. These insights are instrumental in the iterative process of material improvement, aiming to enhance their structural integrity and functional capacity, thereby paving the way for their successful commercialization and broader technological integration [164]. These support materials are expected to significantly extend the catalytic life of the Pt-based systems, ensuring sustainable performance under operational demands.

Table 1 Comparison of different support materials: pros, cons, and applications

Support materials	Pros	Cons	Applications	Ref
Mesoporous carbon	High surface area facilitating better catalyst dispersion, enhanced mass transport due to porous structure	Performance limited under low humidity, Dependency on humidity for optimal performance	Works best under high humidity conditions as the pores facilitate water management within fuel cell membranes	[150, 151]
Graphene	Exceptional electrical conductivity, which enhances electron transfer in ORR	High production cost, Processing challenges, Potential instability in harsh environments	Ideal in environments requiring high conductivity without significant thermal or chemical degradation	[113, 152]
Carbon nanotube	Unique tubular structure provides excellent electron pathways	Difficult dispersion in confined spaces, High cost and processing complexity	Effective in systems where space confinement and conductivity are critical	[153]
Carbon nanofiber	Good mechanical strength and electrical conductivity	High production cost, Complex manufacturing process	Best used where mechanical stability and endurance are valued, such as in automotive applications	[154, 155]
Carbon black	Economically viable and widely available; provides good electrical connectivity	Lower electrical conductivity and catalytic efficiency compared to advanced materials	Suitable for applications where cost-effectiveness is a priority over the highest efficiency	[156]
Metal oxide	Improve the durability of Pt catalysts and introduce unique interaction effects that can enhance ORR activity	Stability issues under high oxidative conditions	Performs well in systems requiring stability under high oxidative environments	[157–159]

For carbon-based supports, they are susceptible to inevitable corrosion issues that significantly undermine their stability and longevity [165–167]. This vulnerability is a critical concern, especially in PEMFCs and other electrochemical systems where durability is essential. The production of CO₂ and CO due to carbon corrosion has several detrimental effects on the catalyst's performance [168]. The depletion of carbon material reduces the structural integrity and mechanical strength of the support, thereby diminishing the overall surface area critical for dispersing and stabilizing catalyst nanoparticles. As carbon support corrodes, Pt nanoparticles may detach and aggregate, resulting in a loss of active surface area and a subsequent decrease in catalytic activity [169]. This detachment is particularly problematic as it directly impacts the ECSA and, consequently, the efficiency of the catalytic process. Furthermore, the generation of CO can poison the catalyst by absorbing onto active Pt sites, further diminishing catalytic activity for reactions such as the ORR and HOR.

To enhance carbon support, it has been noted that doping with impurities can significantly improve the intrinsic ORR activity in fuel cells [170]. Specifically, the incorporation of nitrogen into carbon supports has been extensively researched and applied due to its effectiveness. Nitrogen, which is adjacent to carbon on the periodic table, shares a similar atomic radius with carbon but possesses a distinct electron configuration and electronegativity, making it an ideal dopant [171]. According to the researchers' DFT calculations, the carbon atoms near the nitrogen dopant have a significantly high positive charge density, which counteracts the strong electronegativity of the nitrogen atoms. By modifying the charge of neighboring C atoms, interfacial electron transfer and reactant adsorption are promoted, thereby enhancing the 4e⁻ pathway of ORR. On the other hand, Pt-based ORR catalysts favoring the 4e⁻ pathway can be obtained by modifying the structure of Pt-based NPs without the use of supports, e.g., the compressive strain induced by the alloy core–shell structure can weaken the Pt–O binding energy and increase the 4e⁻ ORR activity [172]. There is also potential for developing a novel alloy core–shell structure, where certain transition metal elements are encapsulated on the surface, with Pt NPs located in the inner layer of the core–shell configuration [173]. This arrangement prevents the dissolution loss of platinum and effectively enhances the durability of the catalyst.

Single atom catalysts (SACs) offer superior activity and selectivity due to their unique atomic environment and strong metal–support interactions, leading to more efficient fuel cell operations with reduced platinum usage [174, 175]. However, challenges remain in ensuring the long-term stability and cost-effectiveness of SACs, directing future research towards innovative synthesis methods and better support materials [176].

Furthermore, it is essential to study Pt-based catalysts under actual fuel cell operating conditions. The efficacy of Pt-based electrodes in electrochemical processes can be influenced by the type of electrode used. Carbon paste electrodes (CPE) are valued for their low background current and easy surface renewal, whereas glassy carbon electrodes (GCE) offer a robust, inert surface with a wide potential range. RDE provides controlled hydrodynamics, enhancing mass transfer and allowing for more precise kinetic studies. Each type impacts the performance and observed activity of Pt-based electrodes, making their choice crucial for specific applications. Future research should focus on understanding and addressing the challenges encountered during fuel cell operations to enhance the performance of Pt-based electrocatalysts. In practical applications, it has been observed that, due to frequent start-up and shut-down (SU/SD) cycles, PEMFCs intermittently experience coexistence of O₂ and H₂ in the anode flow channel [177]. The residual O₂ triggers undesired ORR at the anode, resulting in transient potential jumps and elevating the potential of the cathodic catalyst layer to 1.5–2.0 V. Such conditions accelerate the corrosion of the carbon support material, subsequently degrading the performance of the PEMFC. To enhance the transient stability of fuel cells, it is essential that anode catalysts facilitate the HOR and suppress the ORR at the anode. This necessitates a catalyst that selectively promotes HOR while effectively inhibiting ORR at the anode.

Overview and outlook

This review examines substantial advancements in Pt-based cathode catalysts, emphasizing the role of both carbon and non-carbon supports in augmenting the ORR activity and durability of these catalysts. Furthermore, this review provides insights into the characterization methods for evaluating the ORR performance of Pt-based cathode catalysts, offering guidance for future research activities, such as selecting preparation

methods, tuning element compositions, and optimizing structures to achieve effective ORR catalysts.

The uniform distribution of Pt NPs on the support is crucial for fuel cell performance, as it affects the ECSA and its retention after cycling. To increase the feasibility of using Pt in hydrogen fuel cell vehicles, cost reduction is essential. A promising approach is to enhance the bonding strength between the support and Pt-based NPs, thereby reducing the required Pt loading. Despite these advancements, several key issues warrant further investigation. Understanding the ORR mechanism and the four-electron pathway is essential to address practical challenges in automotive PEMFCs. Based on the current review of Pt-based catalysts, future PEMFC research should consider the following points:

- For carbon support, enhancing the preparation process to increase the degree of graphitization and develop a porous structure can mitigate the impact of carbon corrosion on catalyst performance. Doping carbon composite supports with metal elements at high potential has been shown to improve the selectivity of the four-electron ORR pathway. However, the underlying mechanism driving this selectivity remains unclear. Therefore, further research is urgently needed to fully exploit the efficiency of fuel cells.
- When using metal oxides as non-carbon supports, it is important to consider the mechanism of SMSI, which influences the d-band center value of Pt. Adjusting the composition of metal oxides can optimize the d-band center value for enhanced performance. Beyond TiO_2 , other metal oxides have demonstrated excellent potential as support materials. Future research on SMSI will help identify more suitable metal oxides to further improve the ORR performance of catalysts.
- In the practical application of automotive PEMFCs, it is crucial to develop catalysts that can withstand continuous cycling during SU/SD events. These catalysts should effectively mitigate the anode ORR, promote the HOR, reduce catalyst overpotential, and prevent support corrosion, as well as the detachment and aggregation of Pt NPs in harsh environments. These improvements are essential to extend the service life of fuel cell vehicles.
- Enhancing the morphology and structure of Pt can improve the SA and MA of the catalyst. Several

studies have demonstrated that core–shell structures with a Pt shell layer can significantly enhance Pt utilization by increasing the ECSA. By leveraging the advantages of Pt nanostructures and novel supports, advanced ORR electrocatalysts have been developed, bringing PEMFCs closer to commercial application.

- SACs: The integration of SACs presents a promising frontier. SACs utilize atomic-scale precision to maximize the catalytic efficiency of precious metals like platinum. Future research should focus on optimizing SACs for enhanced stability, exploring new support materials that can maintain single-atom dispersion under operational stresses, and scaling these technologies for commercial deployment.

Acknowledgements

This work was supported by CITIC Dameng Mining Industries Limited-Guangxi University Joint Research Institute of manganese resources utilization and advanced materials technology, Guangxi University-CITIC Dameng Miming Industries Limited Joint base of postgraduate cultivation, and National Natural Science Foundation of China (No.11364003), Guangxi Innovation Driven Development Project (Nos: AA17204100, AA18118052), the Natural Science Foundation of Guangxi Province (No.2018GXNSFAA138186).

Author contributions

Feng Zhan: Writing—original draft, Funding acquisition, Formal analysis, Conceptualization. Lingyun Huang: Writing—original draft, Formal analysis. Yue Luo: Writing—original draft, Formal analysis. Muyang Chen: Writing—review & editing, Formal analysis. Rui Tan: Writing—review & editing, Formal analysis, Supervision. Xinhua Liu: Writing—review & editing, Formal analysis, Supervision. Gang Liu: Writing—original draft, Formal analysis. Zhiming Feng: Formal analysis, Writing—review & editing, Supervision.

Funding

The Funding was provided by National Natural Science Foundation of China, 11364003, Feng Zhan, Guangxi Innovation Driven Development Project, AA17204100, Feng Zhan, AA18118052, Feng Zhan, Natural Science Foundation of Guangxi Province, 2018GXNSFAA138186, Feng Zhan

Data and code availability

Not Applicable.

Declarations

Conflict of interest There are no conflicts to declare.

Ethical approval Not Applicable.

Open Access This article is licensed under a Creative Commons Attribution 4.0 International License, which permits use, sharing, adaptation, distribution and reproduction in any medium or format, as long as you give appropriate credit to the original author(s) and the source, provide a link to the Creative Commons licence, and indicate if changes were made. The images or other third party material in this article are included in the article's Creative Commons licence, unless indicated otherwise in a credit line to the material. If material is not included in the article's Creative Commons licence and your intended use is not permitted by statutory regulation or exceeds the permitted use, you will need to obtain permission directly from the copyright holder. To view a copy of this licence, visit <http://creativecommons.org/licenses/by/4.0/>.

References

- Cullen DA, Neyerlin KC, Ahluwalia RK et al (2021) *Nat Energy* 6:462. <https://doi.org/10.1038/s41560-021-00775-z>
- Jiao K, Xuan J, Du Q et al (2021) *Nature* 595:361. <https://doi.org/10.1038/s41586-021-03482-7>
- Kodama K, Nagai T, Kuwaki A, Jinnouchi R, Morimoto Y (2021) *Nat Nanotechnol* 16:140. <https://doi.org/10.1038/s41565-020-00824-w>
- Y Luo, Y Zhang, J Zhu, et al. (2024) *Small Methods*: e2400158. <https://doi.org/10.1002/smt.202400158>
- Kapse S, Barman N, Thapa R (2023) *Carbon* 201:703. <https://doi.org/10.1016/j.carbon.2022.09.059>
- Feng Z, Eiubovi I, Shao Y, Fan Z, Tan R (2024) *Chain* 1:54. <https://doi.org/10.23919/chain.2024.000001>
- Zhou Z, Zhang H-J, Feng X, Ma Z, Ma Z-F, Xue Y (2024) *J Electroanal Chem* 959:118165. <https://doi.org/10.1016/j.jelechem.2024.118165>
- Kwao S, Vedachalam S, Dalai AK, Adjaye J (2024) *J Ind Eng Chem* 135:1. <https://doi.org/10.1016/j.jiec.2024.01.027>
- Zhang M, Tan R, Wang M, Zhang Z, Low CTJ, Lai Y (2024) *Battery Energy* 3(2):20230050. <https://doi.org/10.1002/bte2.20230050>
- Lai J, Tan R, Jiang H, Huang X, Tian Z, Hong B, Wang M, Li J (2024) *Battery Energy* 3(4):20230070. <https://doi.org/10.1002/bte2.20230070>
- Feng Z, Jin S, Xiang H, Li D, Sun S, Zhang H, Chen Y (2023) *J Polym Res* 30(11):418. <https://doi.org/10.1007/s10965-023-03787-3>
- Ahmadi A, Nezamzadeh-Ejehieh A (2017) *J Electroanal Chem* 801:328. <https://doi.org/10.1016/j.jelechem.2017.08.009>
- Sheikh-Mohseni MH, Nezamzadeh-Ejehieh A (2014) *Electrochim Acta* 147:572. <https://doi.org/10.1016/j.electacta.2014.09.123>
- Alidusty F, Nezamzadeh-Ejehieh A (2016) *Int J Hydrogen Energy* 41:6288. <https://doi.org/10.1016/j.ijhydene.2016.02.149>
- Tohidi MS, Nezamzadeh-Ejehieh A (2016) *Int J Hydrogen Energy* 41:8881. <https://doi.org/10.1016/j.ijhydene.2016.03.106>
- Wang C, Feng Z, Zhao Y et al (2017) *Int J Hydrogen Energy* 42:29988. <https://doi.org/10.1016/j.ijhydene.2017.09.168>
- Li X, Zhao Y, Feng Z et al (2017) *J Membr Sci* 528:55. <https://doi.org/10.1016/j.memsci.2016.12.050>
- Li S, Liao G, Bildan D et al (2024) *Int J Hydrogen Energy* 67:448. <https://doi.org/10.1016/j.ijhydene.2024.04.211>
- Jiahao X, Gao J, Wang H, Suo Y, Zhang Z (2024) *J Electroanal Chem* 966:118401. <https://doi.org/10.1016/j.jelechem.2024.118401>
- Sudarsono W, Tan SY, Wong WY et al (2023) *J Ind Eng Chem* 122:1. <https://doi.org/10.1016/j.jiec.2023.03.004>
- Yang X, Kong W, Guangyuan D, Li S, Tang Y, Cao J, Xueyi L, Tan R, Qian G (2023) *Batteries* 9(9):446. <https://doi.org/10.3390/batteries9090446>
- Li D, Xie S, Liang J, Ma B, Jianing F, Jing W, Feng Y, Feng Z (2024) *Separat Purif Technol* 340:126545. <https://doi.org/10.1016/j.seppur.2024.126545>
- Mohammadi T, Hosseini MG, Pastor E, Ashassi-Sorkhabi H (2024) *J Energy Storage* 79:110146. <https://doi.org/10.1016/j.est.2023.110146>
- Raeisi-Kheirabadi N, Nezamzadeh-Ejehieh A, Aghaei H (2021) *Microchem J* 162:105869. <https://doi.org/10.1016/j.microc.2020.105869>
- Raeisi-Kheirabadi N, Nezamzadeh-Ejehieh A, Aghaei H (2022) *ACS Omega* 7:31413. <https://doi.org/10.1021/acsomega.2c03441>
- Tamiji T, Nezamzadeh-Ejehieh A (2019) *Electrocatalysis* 10:466. <https://doi.org/10.1007/s12678-019-00528-3>
- Tamiji T, Nezamzadeh-Ejehieh A (2019) *Mater Chem Phys* 237:121813. <https://doi.org/10.1016/j.matchemphys.2019.121813>
- Hao H, Tan R, Ye C, Low CTJ (2024). *Carbon Energy*. <https://doi.org/10.1002/cey2.604>
- Rezaei M, Nezamzadeh-Ejehieh A, Massah AR (2024) *Energy Fuels* 38:7637. <https://doi.org/10.1021/acs.energyfuels.4c00325>
- Rezaei M, Nezamzadeh-Ejehieh A, Massah AR (2024) *ACS Omega* 9:6093. <https://doi.org/10.1021/acsomega.3c07560>
- Xing L, Shi W, Su H et al (2019) *Energy* 177:445. <https://doi.org/10.1016/j.energy.2019.04.084>

- [32] Raeisi-Kheirabadi N, Nezamzadeh-Ejehieh A, Aghaei H (2021) Iranian J Catal 11(2):181–189
- [33] Raeisi-Kheirabadi N, Nezamzadeh-Ejehieh A (2022) ChemistrySelect 7(44):e202203788. <https://doi.org/10.1002/slct.202203788>
- [34] Tamiji T, Nezamzadeh-Ejehieh A (2019) J Taiwan Inst Chem Eng 104:130. <https://doi.org/10.1016/j.jtice.2019.08.021>
- [35] Lori O, Elbaz L (2020) ChemCatChem 12:3434. <https://doi.org/10.1002/cctc.202000001>
- [36] Łukaszewski M, Soszko M, Czerwiński A (2023) J Electroanal Chem 929:117060. <https://doi.org/10.1016/j.jelechem.2022.117060>
- [37] Ren X, Wang Y, Liu A, Zhang Z, Lv Q, Liu B (2020) Journal of Materials Chemistry A 8:24284. <https://doi.org/10.1039/d0ta08312g>
- [38] Asset T, Atanassov P (2020) Joule 4:33. <https://doi.org/10.1016/j.joule.2019.12.002>
- [39] He Y, Liu S, Priest C, Shi Q, Wu G (2020) Chem Soc Rev 49:3484. <https://doi.org/10.1039/c9cs00903e>
- [40] Mai J, Zhang Y, He H, Luo Y, Zhou X, Kunsong H, Liu G, Sugumar MK, Low CTJ, Liu X, Tan R (2024) Mater Today Chem 38:102079. <https://doi.org/10.1016/j.mtchem.2024.102079>
- [41] Liu X, Yang W, Chen L et al (2020) ACS Appl Mater Interfaces 12:4463. <https://doi.org/10.1021/acsami.9b18454>
- [42] Zhou X, Liu X, Zhang J et al (2020) Carbon 166:284. <https://doi.org/10.1016/j.carbon.2020.05.037>
- [43] Berber MR, Alenad AM, Althubiti NA, Alrowaili ZA, Zahran ZN, Yagi M (2022) Fuel 312:122954. <https://doi.org/10.1016/j.fuel.2021.122954>
- [44] Xiao F, Wang Q, Xu G-L et al (2022) Nat Catal 5:503. <https://doi.org/10.1038/s41929-022-00796-1>
- [45] Li S, Xin Z, Han J et al (2024). Ionics. <https://doi.org/10.1007/s11581-024-05778-w>
- [46] Biz C, Fianchini M, Polo V, Gracia J (2020) ACS Appl Mater Interfaces 12:50484. <https://doi.org/10.1021/acsami.0c15353>
- [47] Zonghua P, Cheng R, Zhao J, Zhiyi H, Li C, Li W, Wang P, Amiin IS, Wang Z, Wang M, Chen D, Shichun M (2020) iScience 23(12):101793. <https://doi.org/10.1016/j.isci.2020.101793>
- [48] Ao X, Zhang W, Zhao B et al (2020) Energy Environ Sci 13:3032. <https://doi.org/10.1039/d0ee00832j>
- [49] Hu Y, Guo X, Shen T, Zhu Y, Wang D (2022) ACS Catal 12:5380. <https://doi.org/10.1021/acscatal.2c01541>
- [50] Jung JY, Kim D-g, Jang I, Kim ND, Yoo SJ, Kim P (2022) J Indust Eng Chem 111:300–307. <https://doi.org/10.1016/j.jiec.2022.04.011>
- [51] Sun W, Li T, Chu H, Liu J, Feng L (2022) Fuel 329:125410. <https://doi.org/10.1016/j.fuel.2022.125410>
- [52] Wan C, Duan X, Huang Y (2020) Adv Energy Mater 10:14. <https://doi.org/10.1002/aenm.201903815>
- [53] Song Z, Zhu YN, Liu H et al (2020) Small 16:e2003096. <https://doi.org/10.1002/sml.202003096>
- [54] Guo Z, Shi T, Yu S et al (2024) J Mater Sci 59:1380. <https://doi.org/10.1007/s10853-023-09292-8>
- [55] Kumar S, Yen-Pei F (2023) J Energy Storage 62:106862. <https://doi.org/10.1016/j.est.2023.106862>
- [56] Du L, Prabhakaran V, Xie X, Park S, Wang Y, Shao Y (2021) Adv Mater 33:e1908232. <https://doi.org/10.1002/adma.201908232>
- [57] Yang L, Shui J, Du L et al (2019) Adv Mater 31:e1804799. <https://doi.org/10.1002/adma.201804799>
- [58] Mohideen MM, Liu Y, Ramakrishna S (2020) Appl Energy 257:114027. <https://doi.org/10.1016/j.apenergy.2019.114027>
- [59] Tripkovic V, Vegge T (2017) J Phys Chem C 121:26785. <https://doi.org/10.1021/acs.jpcc.7b07472>
- [60] Liu Z, Tan H, Li B et al (2023) Nat Commun 14:3374. <https://doi.org/10.1038/s41467-023-38914-7>
- [61] Yan T, Lang S, Liu S et al (2024) J Colloid Interface Sci 669:32. <https://doi.org/10.1016/j.jcis.2024.04.161>
- [62] Lin SC, Chang CW, Tsai MH, Chen CH, Lin JT, Wu CY, Kao IT, Jao WY, Wang CH, Yu WY, Hu CC (2024) Adv Funct Mater 34:2314281. <https://doi.org/10.1002/adfm.202314281>
- [63] Stamoulis AG, Bruns DL, Stahl SS (2023) J Am Chem Soc 145:17515. <https://doi.org/10.1021/jacs.3c02887>
- [64] Ji S, Mou Y, Liu H et al (2024) Adv Mater 36:e2410121. <https://doi.org/10.1002/adma.202410121>
- [65] Zhang H, Chen HC, Feizpoor S et al (2024) Adv Mater 36:e2400523. <https://doi.org/10.1002/adma.202400523>
- [66] Nørskov JK, Rossmeisl J, Logadottir A, Lindqvist LRKJ, Kitchin JR, Bligaard T, Jonsson H (2004) J Phys Chem B 108(46):17886–17892
- [67] Kitchin JR, Nørskov JK, Barteau MA, Chen JG (2004) J Chem Phys 120:10240. <https://doi.org/10.1063/1.1737365>
- [68] Feng Z, Gupta G, Mamlouk M (2023) Int J Hydrogen Energy 48:25830. <https://doi.org/10.1016/j.ijhydene.2023.03.299>
- [69] Huang J, Zhu X, Eikerling M (2021) Electrochim Acta 393:139019. <https://doi.org/10.1016/j.electacta.2021.139019>
- [70] Kato M, Iguchi Y, Li T et al (2021) ACS Catal 12:259. <https://doi.org/10.1021/acscatal.1c04597>
- [71] Röttcher NC, Yu-Ping K, Minichova M, Ehelebe K, Cherevko S (2023) J Phys: Energy 5(2):024007. <https://doi.org/10.1088/2515-7655/acbe1b>
- [72] Della Bella RKF, Stühmeier BM, Gasteiger HA (2022) J Electrochem Soc 169(4):044528. <https://doi.org/10.1149/1945-7111/ac67b8>
- [73] Jingsong Xu, Li R, Cong-Qiao X, Zeng R, Jiang Z, Mei B, Li J, Meng D, Chen J (2021) Appl Catal B: Environ 289:120028. <https://doi.org/10.1016/j.apcatb.2021.120028>
- [74] Gomes BF, Prokop M, Bystron T, Loukrakpam R, Lobo CMS, Kutter M, Günther TE, Fink M, Bouzek K, Roth C (2022) J Electroanal Chem 918:116450. <https://doi.org/10.1016/j.jelechem.2022.116450>
- [75] Kerschbaumer A, Wielend D, Leeb E et al (2023) Catal Sci Technol 13:834. <https://doi.org/10.1039/d2cy01744j>
- [76] Riasse R, Lafforgue C, Vandenberghe F, Micoud F, Morin A, Arenz M, Durst J, Chatenet M (2023) J Power Sour 556:232491. <https://doi.org/10.1016/j.jpowsour.2022.232491>
- [77] Lilloja J, Kibena-Pöldsepp E, Sarapuu A, Käärik M, Kozlova J, Paiste P, Kikas A, Treshchalov A, Leis J, Tamm A, Kisand V, Holdcroft S, Tammeveski K (2022) Appl Catal B: Environ 306:121113. <https://doi.org/10.1016/j.apcatb.2022.121113>
- [78] Lilloja J, Kibena-Pöldsepp E, Sarapuu A, Kikas A, Kisand V, Käärik M, Merisalu M, Treshchalov A, Leis J, Sammelselg V, Wei Q, Holdcroft S, Tammeveski K (2020) Appl Catal B: Environ 272:119012. <https://doi.org/10.1016/j.apcatb.2020.119012>
- [79] Zamora JA, Zeledón GA, Kamat GT, Gunasooriya KK, Nørskov JK, Stevens MB, Jaramillo TF (2021) ChemElectroChem 8(13):2467–2478. <https://doi.org/10.1002/celec.202100500>
- [80] Beermann V, Holtz ME, Padgett E, de Araujo JF, Muller DA, Strasser P (2019) Energy Environ Sci 12:2476. <https://doi.org/10.1039/c9ee01185d>
- [81] Ziabari A, Rahman O, Yu H, Arregui-Mena JD, Venkatakrisnan SV, Cullen DA (2023) Microsc Microanal 29:1385. <https://doi.org/10.1093/micmic/ozad067.713>
- [82] Liu S, Lin R, Jiapeng L, Wang Y, Cai X (2023) Chem Eng J 472:145050. <https://doi.org/10.1016/j.cej.2023.145050>

- [83] Feng Z, Gupta G, Mamlouk M (2024) *J Appl Polym Sci* 141(19):55340. <https://doi.org/10.1002/app.55340>
- [84] Ponomarev II, Skupov KM, Naumkin AV, Basu VG, Zhigalina OM, Razorenov DY, Ponomarev II, Volkova YA (2019) *RSC Adv* 9(1):257–267. <https://doi.org/10.1039/C8RA07177B>
- [85] Morales DM, Kazakova MA, Dieckhöfer S, Selyutin AG, Golubtsov GV, Schuhmann W, Masa J (2019) *Adv Funct Mater* 30(6):1905992. <https://doi.org/10.1002/adfm.201905992>
- [86] Stonkus O, Kibis L, Slavinskaya E, Zadesenets A, Garkul I, Kardash T, Stadnichenko A, Korenev S, Podyacheva O, Boronin A (2023) *Materials* 16(12):4257. <https://doi.org/10.3390/ma16124257>
- [87] Li D, Liu J, Chen X, Feng Z, Wang S, Wang Y, Lin N, Jing W, Feng Y (2025) *Appl Catal B: Environ Energy* 365:124824. <https://doi.org/10.1016/j.apcatb.2024.124824>
- [88] Torabi M, Tomapatanaget B, Shervedani RK (2024) *J Mater Sci* 59(17):7218–7234. <https://doi.org/10.1007/s10853-024-09587-4>
- [89] Prithi JA, Vedarajan R, Ranga Rao G, Rajalakshmi N (2021) *Int J Hydrogen Energy* 46(34):17871–17885. <https://doi.org/10.1016/j.ijhydene.2021.02.186>
- [90] Li Y, Wang F, Zhu H (2020) *J Mater Sci* 55:11241. <https://doi.org/10.1007/s10853-020-04808-y>
- [91] Zhao W, Ye Y, Jiang W et al (2020) *J Mater Chem A* 8:15822. <https://doi.org/10.1039/d0ta01437k>
- [92] Su H, Hu YH (2020) *Energy Sci Eng* 9:958. <https://doi.org/10.1002/ese3.833>
- [93] Saadat N, Dhakal HN, Tjong J, Jaffer S, Yang W, Sain M (2021) *Renew Sustain Energy Rev* 138:110535. <https://doi.org/10.1016/j.rser.2020.110535>
- [94] Peera SG, Koutavarapu R, Akula S et al (2021) *Energy Fuels* 35:11761. <https://doi.org/10.1021/acs.energyfuels.1c01439>
- [95] Zasyapkina AA, Ivanova NA, Spasov DD, Mensharapov RM, Alekseeva OK, Vorobyeva EA, Kukueva EV, Fateev VN (2023) *Inorganics* 11(5):219. <https://doi.org/10.3390/inorg11050219>
- [96] Ortíz-Herrera JC, Tellez-Cruz MM, Solorza-Feria O, Medina DI (2022) *Catalysts* 12(5):477. <https://doi.org/10.3390/catal12050477>
- [97] Zhao J, Zhengkai T, Chan SH (2021) *J Power Sour* 488:229434. <https://doi.org/10.1016/j.jpowsour.2020.229434>
- [98] Borup RL, Kusoglu A, Neyerlin KC et al (2020) *Curr Opin Electrochem* 21:192. <https://doi.org/10.1016/j.coelec.2020.02.007>
- [99] Cheng N, Zhang L, Zhou Y et al (2020) *J Colloid Interface Sci* 572:170. <https://doi.org/10.1016/j.jcis.2020.03.083>
- [100] Ehelebe K, Knoppel J, Bierling M et al (2021) *Angew Chem Int Ed Engl* 60:8882. <https://doi.org/10.1002/anie.202014711>
- [101] Jayabal S, Saranya G, Geng D, Lin L-Y, Meng X (2020) *Journal of Materials Chemistry A* 8:9420. <https://doi.org/10.1039/d0ta01530j>
- [102] Ando F, Gunji T, Tanabe T et al (2021) *ACS Catal* 11:9317. <https://doi.org/10.1021/acscatal.1c01868>
- [103] Li X, Liu Q, Yang B, Liao Z, Yan W, Xiang Z (2022) *Adv Mater* 34:e2204570. <https://doi.org/10.1002/adma.202204570>
- [104] Xiong W, Yin H, Wu T, Li H (2023) *Chemistry* 29:e202202872. <https://doi.org/10.1002/chem.202202872>
- [105] Gu K, Kim EJ, Sharma SK, Sharma PR, Bliznakov S, Hsiao BS, Rafailovich MH (2021) *Mater Today Energy* 19:100560. <https://doi.org/10.1016/j.mtener.2020.100560>
- [106] Yang Y, Wang Z, Mai Y et al (2021) *J Mater Sci* 56:13083. <https://doi.org/10.1007/s10853-021-06159-8>
- [107] Liao Y, Wang Y, Liu J, Tang Y, Wu C, Chen Y (2021) *Ind Eng Chem Res* 60:14728. <https://doi.org/10.1021/acs.iecr.1c03533>
- [108] Li Y, Gui F, Wang F, Liu J, Zhu H (2021) *Int J Hydrogen Energy* 46:37802. <https://doi.org/10.1016/j.ijhydene.2021.09.042>
- [109] Ionescu V, Balan A, Trefilov A, Stamatin I (2021) *Energies* 14(19):6232. <https://doi.org/10.3390/en14196232>
- [110] Tian LL, Yang J, Weng MY et al (2017) *ACS Appl Mater Interfaces* 9:7125. <https://doi.org/10.1021/acsami.6b15235>
- [111] Zhao Z, Liu Z, Zhang A et al (2022) *Nat Nanotechnol* 17:968. <https://doi.org/10.1038/s41565-022-01170-9>
- [112] Liu J, Ma Q, Huang Z, Liu G, Zhang H (2019) *Adv Mater* 31:e1800696. <https://doi.org/10.1002/adma.201800696>
- [113] Jaimes-Paez CD, Morallón E, Cazorla-Amorós D (2023) *Energy* 278:127888. <https://doi.org/10.1016/j.energy.2023.127888>
- [114] Han J, Lee H, Kim J, Kim S, Kim H, Kim E, Sung Y-E, Kim K, Lee J-C (2020) *J Membr Sci* 612:118428. <https://doi.org/10.1016/j.memsci.2020.118428>
- [115] Ohma A, Furuya Y, Mashio T, Ito M, Nomura K, Nagao T, Nishihara H, Jinnai H, Kyotani T (2021) *Electrochim Acta* 370:137705. <https://doi.org/10.1016/j.electacta.2020.137705>
- [116] Marinoiu A, Raceanu M, Andrulevicius M et al (2020) *Arab J Chem* 13:3585. <https://doi.org/10.1016/j.arabjc.2018.12.009>
- [117] Pushkareva IV, Pushkarev AS, Kalinichenko VN, Chumakov RG, Soloviev MA, Liang Y, Millet P, Grigoriev SA (2021) *Catalysts* 11(2):256. <https://doi.org/10.3390/catal11020256>
- [118] Sravani B, Reddy YVM, Park JP, Venu M, Sarma LS (2022) *Catalysts* 12(12):1528. <https://doi.org/10.3390/catal12121528>
- [119] Haque MA, Rahman MM, Islam F et al (2023) *Energies* 16(3):1537. <https://doi.org/10.3390/en16031537>
- [120] Wei P, Li X, He Z et al (2021) *Chem Eng J* 422:130134. <https://doi.org/10.1016/j.cej.2021.130134>
- [121] Sasaki T, Izumi R, Tsuda T, Kuwabata S (2021) *ACS Appl Energy Mater* 4:7298. <https://doi.org/10.1021/acsaem.1c01410>
- [122] Yao Y, Xiao Q, Kawaguchi M, Tsuda T, Yamada H, Kuwabata S (2022) *RSC Adv* 12:14268. <https://doi.org/10.1039/d2ra01330d>
- [123] Mardle P, Ji X, Jing W, Guan S, Dong H, Shangfeng Du (2020) *Appl Catal B: Environ* 260:118031. <https://doi.org/10.1016/j.apcatb.2019.118031>
- [124] Ortiz-Herrera JC, Cruz-Martínez H, Solorza-Feria O, Medina DI (2022) *Int J Hydrogen Energy* 47:30213. <https://doi.org/10.1016/j.ijhydene.2022.03.218>
- [125] Marbaniang P, Ingavale S, Karuppanan P, Swami A, Kakade B (2021) *Int J Hydrogen Energy* 46:10268. <https://doi.org/10.1016/j.ijhydene.2020.12.121>
- [126] Pei Y, Song H, Liu Y et al (2021) *J Colloid Interface Sci* 600:865. <https://doi.org/10.1016/j.jcis.2021.05.089>
- [127] Vinothkannan M, Kim AR, Ramakrishnan S, Yeon-Tae Y, Yoo DJ (2021) *Compos Part B: Eng* 215:108828. <https://doi.org/10.1016/j.compositesb.2021.108828>
- [128] Waldrop K, Wycisk R, Pintauro PN (2020) *Curr Opin Electrochem* 21:257. <https://doi.org/10.1016/j.coelec.2020.03.007>
- [129] Chung S, Ham K, Kang S, HyungKuk J, Lee J (2020) *Electrochim Acta* 348:136346. <https://doi.org/10.1016/j.electacta.2020.136346>
- [130] Akula S, Sahu AK (2020) *ACS Appl Mater Interfaces* 12:11438. <https://doi.org/10.1021/acsaami.9b18790>
- [131] Dahal B, Chae S-H, Muthurasu A, Mukhiya T, Gautam J, Chhetri K, Subedi S, Ojha GP, Tiwari AP, Lee JH, Kim H-Y (2020) *J Power Sour* 453:227883. <https://doi.org/10.1016/j.jpowsour.2020.227883>
- [132] Akula S, Varathan P, Kesh A et al (2022) *Int J Hydrogen Energy* 47:20617. <https://doi.org/10.1016/j.ijhydene.2022.04.163>
- [133] Zhou T, Zhang J, Yang S, Jin J, Wang B, Li G (2022) *Materials* 15(13):4560. <https://doi.org/10.3390/ma15134560>

- [134] Ji Z, Chen J, Pérez-Page M et al (2022) *J Energy Chem* 68:143. <https://doi.org/10.1016/j.jechem.2021.09.031>
- [135] Mladenović D, Santos DMF, Bozkurt G, Soylu GSP, Yurtcan AB, Mišćević Š, Šljukić B (2021) *Electrochem Commun* 124:106963. <https://doi.org/10.1016/j.elecom.2021.106963>
- [136] Ayyubov I, Tálas E, Salmazadeh K, Kuncser A, Pászti Z, Neațu Ș, Mirea AG, Florea M, Tompos A, Borbáth I (2022) *Materials* 15(10):3671. <https://doi.org/10.3390/ma15103671>
- [137] Salesi S, Nezamzadeh-Ejhi A (2023) *Environ Sci Pollut Res Int* 30:105440. <https://doi.org/10.1007/s11356-023-29730-z>
- [138] Zabihi-Mobarakeh H, Nezamzadeh-Ejhi A (2015) *J Ind Eng Chem* 26:315. <https://doi.org/10.1016/j.jiec.2014.12.003>
- [139] Nezamzadeh-Ejhi A, Bahrami M (2015) *Desalin Water Treat* 55:1096. <https://doi.org/10.1080/19443994.2014.922443>
- [140] Ma Y, Nagai T, Inoue Y et al (2021) *Mater Des* 203:109623. <https://doi.org/10.1016/j.matdes.2021.109623>
- [141] Diczházi D, Borbáth I, Bakos I, Szijjártó GP, Tompos A, Pászti Z (2021) *Catal Today* 366:31. <https://doi.org/10.1016/j.cattod.2020.04.004>
- [142] Borbáth I, Zelenka K, Vass Á et al (2021) *Int J Hydrogen Energy* 46:13534. <https://doi.org/10.1016/j.ijhydene.2020.08.002>
- [143] Kong J, Qin Y-H, Wang T-L, Wang C-W (2020) *Int J Hydrogen Energy* 45:1991. <https://doi.org/10.1016/j.ijhydene.2019.11.016>
- [144] Park C, Lee E, Lee G, Tak Y (2020) *Appl Catal B: Environ* 268:118414. <https://doi.org/10.1016/j.apcatb.2019.118414>
- [145] You S-H, Jung S-M, Kim K-S et al (2023) *ACS Energy Lett* 8:2201. <https://doi.org/10.1021/acseenergylett.2c02656>
- [146] Ghattavi S, Nezamzadeh-Ejhi A (2020) *Int J Hydrogen Energy* 45:24636. <https://doi.org/10.1016/j.ijhydene.2020.06.207>
- [147] Ghattavi S, Nezamzadeh-Ejhi A (2020) *Compos Part B: Eng* 183:107712. <https://doi.org/10.1016/j.compositesb.2019.107712>
- [148] Raeisi-Kheirabadi N, Nezamzadeh-Ejhi A (2020) *Int J Hydrogen Energy* 45:33381. <https://doi.org/10.1016/j.ijhydene.2020.09.028>
- [149] Foroughipour M, Nezamzadeh-Ejhi A (2023) *Chemosphere* 334:139019. <https://doi.org/10.1016/j.chemosphere.2023.139019>
- [150] Collins G, Kasturi PR, Karthik R, Shim J-J, Sukanya R, Breslin CB (2023) *Electrochim Acta* 439:141678. <https://doi.org/10.1016/j.electacta.2022.141678>
- [151] Zhang F, Liu X, Chen Y, Tian M, Yang T, Zhang J, Gao S (2023) *Chinese Chem Lett* 34(10):108142. <https://doi.org/10.1016/j.ccllet.2023.108142>
- [152] Bhaskaran R, Chetty R (2024) *ACS Appl Energy Mater* 7:390. <https://doi.org/10.1021/acsaem.3c01956>
- [153] Lu Z, Xiong Q, Fu R et al (2024) *Int J Hydrogen Energy* 61:203. <https://doi.org/10.1016/j.ijhydene.2024.02.283>
- [154] Han J, Deng N, Chi H et al (2024) *J Energy Chem* 98:334. <https://doi.org/10.1016/j.jechem.2024.06.051>
- [155] Jaimes-Paez CD, García-Mateos FJ, Ruiz-Rosas R, Rodríguez-Mirasol J, Cordero T, Morallón E, Cazorla-Amorós D (2023) *Nanomaterials* 13(22):2921. <https://doi.org/10.3390/nano13222921>
- [156] Bai F, Zhang Y, Hou D et al (2024) *J Mater Chem A* 12:384. <https://doi.org/10.1039/d3ta04599d>
- [157] Fasulo F, Massaro A, Pecoraro A, Muñoz-García AB, Pavone M (2023) *Curr Opin Electrochem* 42:101412. <https://doi.org/10.1016/j.coelec.2023.101412>
- [158] Wang S, Wang M, Zhang Y et al (2023) *Small Methods* 7:e2201714. <https://doi.org/10.1002/smt.202201714>
- [159] Zheng J, Meng D, Guo J, Liu X, Zhou L, Wang Z (2024) *Adv Mater* 36:e2405129. <https://doi.org/10.1002/adma.202405129>
- [160] Qiu Y, Wu Y, Wei X et al (2024) *Nano Lett* 24:9034. <https://doi.org/10.1021/acs.nanolett.4c02178>
- [161] Jiang Y, Haili X, Ma B, Zhang Z, Zhou Y (2024) *Fuel* 366:131404. <https://doi.org/10.1016/j.fuel.2024.131404>
- [162] Feng Z, Gupta G, Mamlouk M (2023) *RSC Adv* 13:20235. <https://doi.org/10.1039/d3ra02889e>
- [163] Sun Z, Zhong Y, Sui H et al (2024). *Adv Func Mater*. <https://doi.org/10.1002/adfm.202410774>
- [164] Li X, Duan X, Zhang S et al (2024) *Angew Chem Int Ed Engl* 63:e202400549. <https://doi.org/10.1002/anie.202400549>
- [165] Wang Y, Hao J, Liu Y et al (2023) *J Energy Chem* 76:601. <https://doi.org/10.1016/j.jechem.2022.09.047>
- [166] Quílez-Bermejo J, García-Dalí S, Daouli A, Zitolo A, Canevesi RL, Emo M, Izquierdo MT, Badawi M, Celzard A, Fierro V (2023) *Adv Funct Mater* 33(21):2300405. <https://doi.org/10.1002/adfm.202300405>
- [167] Campos-Roldán CA, Chattot R, Filhol J-S, Guesmi H, Romero N, Bacabe R, Blanchard P-Y, Vinci V, Drnec J, Rozière J, Jones DJ, Cavaliere S (2024) *ACS Catal* 14(16):11941–11948
- [168] Li XF, Su FY, Xie LJ et al (2024) *Small* 20:32. <https://doi.org/10.1002/sml.202310940>
- [169] Liu P, Li B, Yang D, Zhang C, Ming P (2023) *J Power Sour* 556:232427. <https://doi.org/10.1016/j.jpowsour.2022.232427>
- [170] Sun C, Wen R, Qin Y et al (2023) *ACS Appl Energy Mater* 6:5700. <https://doi.org/10.1021/acsaem.3c00027>
- [171] Zhang BB, Ming J, Li HQ, Song XN, Wang CK, Hua W, Ma Y (2023) *Carbon* 214:118301. <https://doi.org/10.1016/j.carbon.2023.118301>
- [172] Zhang D, Ding R, Shi S, He Y (2023) *Int J Hydrogen Energy* 48:30391. <https://doi.org/10.1016/j.ijhydene.2023.04.161>
- [173] Liu J, Li ZP, Liu BH (2023) *J Alloys Compd* 944:169166. <https://doi.org/10.1016/j.jallcom.2023.169166>
- [174] Sun T, Zang W, Sun J, Li C, Fan J, Liu E, Wang J (2023) *Adv Funct Mater* 33(30):2301526. <https://doi.org/10.1002/adfm.202301526>
- [175] Li S, Xin Z, Luo Y et al (2024) *Int J Hydrogen Energy* 82:1081. <https://doi.org/10.1016/j.ijhydene.2024.08.026>
- [176] Zhang H, Liu G, Shi L, Ye J (2018) *Adv Energy Mater* 8(1):1701343. <https://doi.org/10.1002/aenm.201701343>
- [177] Huang G, Li Y, Tao L et al (2023) *Angew Chem Int Ed Engl* 62:e202215177. <https://doi.org/10.1002/anie.202215177>

Publisher's Note Springer Nature remains neutral with regard to jurisdictional claims in published maps and institutional affiliations.